

The Innate Immune Receptors TLR2/4 Mediate Repeated Social Defeat Stress-Induced Social Avoidance through Prefrontal Microglial Activation

Highlights

- Repeated stress activates mPFC microglia through innate immune receptors TLR2/4
- Activated microglia induce response attenuation and atrophy of mPFC neurons
- Activated microglia underlie repeated stress-induced social avoidance
- TLR2/4 induce IL-1 α and TNF- α in mPFC microglia, leading to social avoidance

Authors

Xiang Nie, Shihō Kitaoka,
Kohei Tanaka, ..., Akira Kakizuka,
Shuh Narumiya, Tomoyuki Furuyashiki

Correspondence

snaru@mfour.med.kyoto-u.ac.jp (S.N.),
tfuruya@med.kobe-u.ac.jp (T.F.)

In Brief

Nie et al. identify TLR2/4 as crucial mediators of repeated stress-induced microglial activation in the mPFC, which leads to neuronal and behavioral changes through inflammation-related cytokines. These results highlight pivotal roles of innate immunity in the mPFC in repeated stress.



The Innate Immune Receptors TLR2/4 Mediate Repeated Social Defeat Stress-Induced Social Avoidance through Prefrontal Microglial Activation

Xiang Nie,^{1,2,3,8,9} Shiho Kitaoka,^{1,8,9} Kohei Tanaka,^{2,9} Eri Segi-Nishida,⁴ Yuki Imoto,⁵ Atsubumi Ogawa,² Fumitake Nakano,¹ Ayaka Tomohiro,^{1,2} Kazuki Nakayama,^{1,2} Masayuki Taniguchi,^{1,8} Yuko Mimori-Kiyosue,⁶ Akira Kakizuka,³ Shuh Narumiya,^{2,7,*} and Tomoyuki Furuyashiki^{1,8,10,*}

¹Division of Pharmacology, Kobe University Graduate School of Medicine, Kobe, Hyogo 650-0017, Japan

²CREST Project, Medical Innovation Center, Kyoto University Graduate School of Medicine, Kyoto, Kyoto 606-8509, Japan

³Laboratory of Functional Biology, Kyoto University Graduate School of Biostudies, Kyoto, Kyoto 606-8501, Japan

⁴Department of Biological Science and Technology, Faculty of Industrial Science and Technology, Tokyo University of Science, Katsushika-ku, Tokyo 125-8585, Japan

⁵Department of Physiological Chemistry, Kyoto University Graduate School of Pharmaceutical Sciences, Kyoto, Kyoto 606-8304, Japan

⁶Laboratory for Molecular and Cellular Dynamics, RIKEN Center for Biosystems Dynamics Research, Kobe, Hyogo 650-0047, Japan

⁷Department of Drug Discovery Medicine, Kyoto University Graduate School of Medicine, Kyoto, Kyoto 606-8507, Japan

⁸AMED-CREST, Chiyoda-ku, Tokyo 100-0004, Japan

*These authors contributed equally

¹⁰Lead Contact

*Correspondence: snaru@mfour.med.kyoto-u.ac.jp (S.N.), tfuruya@med.kobe-u.ac.jp (T.F.)

<https://doi.org/10.1016/j.neuron.2018.06.035>

SUMMARY

Repeated environmental stress has been proposed to induce neural inflammation together with depression and anxiety. Innate immune receptors, such as Toll-like receptors (TLRs), are activated by exogenous or endogenous ligands to evoke inflammation. Here we show that the loss of TLR2 and TLR4 (TLR2/4) abolished repeated social defeat stress (R-SDS)-induced social avoidance and anxiety in mice. TLR2/4 deficiency mitigated R-SDS-induced neuronal response attenuation, dendritic atrophy, and microglial activation in the medial prefrontal cortex (mPFC). Furthermore, mPFC microglia-specific TLR2/4 knockdown blocked social avoidance. Transcriptome analyses revealed that R-SDS induced IL-1 α and TNF- α in mPFC microglia in a TLR2/4-dependent manner, and antibody blockade of these cytokines in the mPFC suppressed R-SDS-induced social avoidance. These results identify TLR2/4 as crucial mediators of R-SDS-induced microglial activation in the mPFC, which leads to neuronal and behavioral changes through inflammation-related cytokines, highlighting unexpected pivotal roles of innate immunity in the mPFC in repeated environmental stress-induced behavioral changes.

INTRODUCTION

Repeated environmental stress induces maladaptive behavioral changes, including depression and anxiety, and is a risk factor

for various human psychiatric disorders (Duman and Aghajanian, 2012; Krishnan and Nestler, 2008; McEwen and Morrison, 2013). To elucidate these mechanisms, rodent models of repeated environmental stress, such as repeated social defeat stress (R-SDS), repeated restraint stress, and chronic unpredictable stress, have been frequently used. In these models, repeated environmental stress alters the morphologies and activities of neurons in multiple brain areas involved in emotional and cognitive functions (Duman and Aghajanian, 2012; McEwen and Morrison, 2013). Among these brain areas, certain areas, such as the medial prefrontal cortex (mPFC) and *nucleus accumbens* (NAc), play pivotal roles in regulating repeated environmental stress-induced behavioral changes. Various kinds of repeated environmental stresses reduce excitatory synaptic transmission and attenuate the environmental stress-induced response of mPFC pyramidal neurons (Ota et al., 2014; Perrotti et al., 2004). Shortening and reduced branching of dendrites as well as the loss of dendritic spines are also induced (Dias-Ferreira et al., 2009; Duman and Aghajanian, 2012; McEwen and Morrison, 2013). These neuronal changes are thought to be responsible for repeated environmental stress-induced depression-like behaviors, such as anhedonia and social avoidance (Golden et al., 2013; Li et al., 2011). Histological and brain imaging studies have reported reduced gray matter volumes and abnormal metabolic activities in the mPFCs of psychiatric patients (Drevets et al., 2008). However, the underlying mechanism whereby repeated environmental stress induces alterations in the morphologies and activities of mPFC neurons as well as consequent behavioral changes remains unknown.

Although the majority of studies have examined neuronal plasticity, which underlies repeated environmental stress-induced behavioral changes, several laboratories, including ours, have focused on neural inflammation or microglial activation as potential mechanisms of repeated environmental stress (Frank et al.,



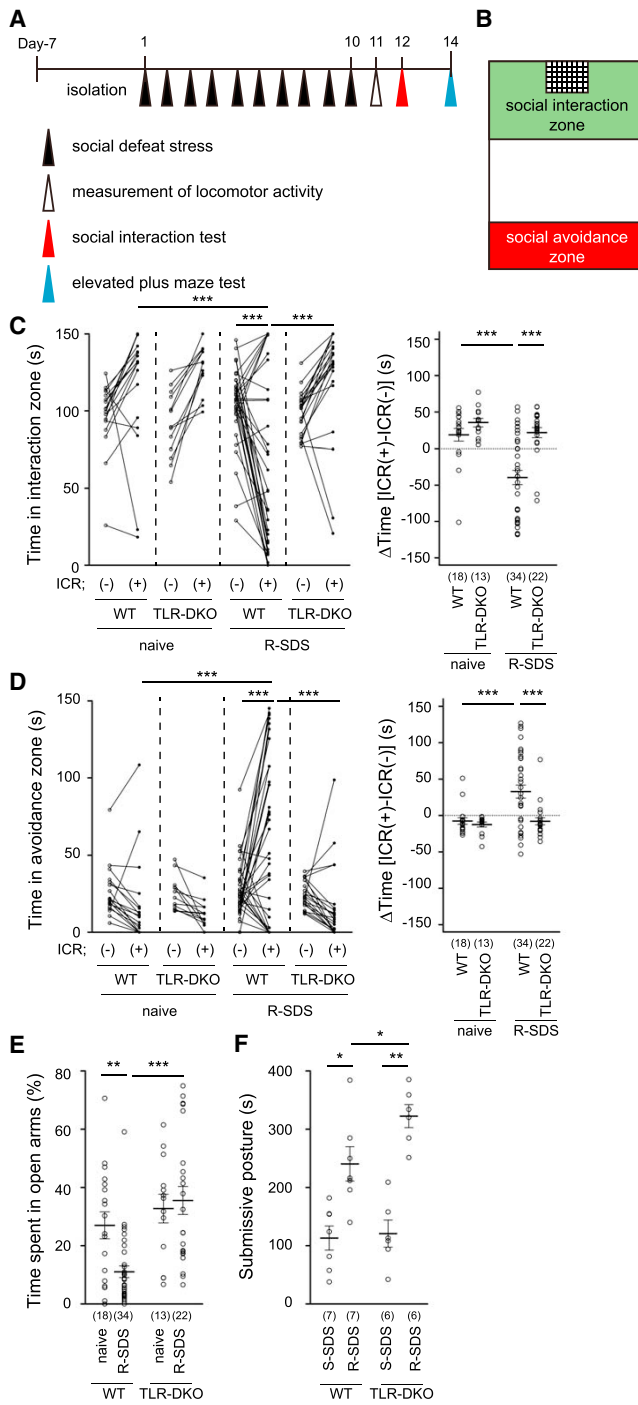


Figure 1. TLR2/4 Are Crucial for R-SDS-Induced Social Avoidance

(A) Schedule of behavioral experiments.

(B) Definitions of the social interaction zone and the social avoidance zone (green and red rectangles, respectively).

(C and D) The levels of social interaction (C) and social avoidance (D) in wild-type (WT) mice and TLR-DKO mice with or without prior R-SDS (R-SDS or naive, respectively). The durations in the interaction (C) or avoidance (D) zone without and with an ICR mouse and the differences between these durations without and with an ICR mouse (Δ Time [ICR(+)-ICR(-)]) were analyzed and are shown.

2007; Giovanoli et al., 2013; Hinwood et al., 2012; Kreisel et al., 2014; Tanaka et al., 2012; Wohleb et al., 2011, 2013). Indeed, genetic deletion of inflammation-related molecules and administration of a drug (minocycline) that potentially affects microglial properties have been shown to attenuate behavioral changes that are concomitant with microglial activation and/or monocyte infiltration in the brain and induced by repeated environmental stress. However, because none of these studies have selectively manipulated microglia or gene expression in microglia, direct evidence demonstrating a role of microglia in repeated environmental stress-induced behavioral changes is lacking.

Microglia can be activated by various extracellular stimuli, many of which are mediated by Toll-like receptors (TLRs) (Rivest, 2009). TLRs have been identified as pattern recognition receptors for pathogen-associated molecular patterns and mediate inflammation and immune responses upon infection. In addition, recent studies have pointed to crucial roles of TLRs in diseases of the brain and other organs without apparent infection (Iwasaki and Medzhitov, 2010; Rivest, 2009) and have proposed that endogenous molecules are released from cells upon cellular damage or stress and act as endogenous ligands for TLRs for inflammation and tissue remodeling.

To identify R-SDS-induced changes in gene expression profiles in the mPFC, we performed a transcriptome analysis and obtained results suggesting that R-SDS upregulates potential ligands for TLR2 and TLR4 in the mPFC. Based on this finding, we analyzed the roles of TLR2 and TLR4 in R-SDS and found that genetic deletion of TLR2 and TLR4 (TLR2/4) in combination abolishes R-SDS-induced social avoidance in mice. R-SDS induced microglial activation and altered neuronal c-Fos expression and morphologies in the mPFC, and TLR2/4 deletion mitigated these changes. Furthermore, we developed a method to manipulate gene expression in microglia in a specific brain area and provide sound evidence, for the first time, that TLR2/4 in mPFC microglia are crucial for R-SDS-induced social avoidance.

RESULTS

TLR2/4 Are Crucial for R-SDS-Induced Social Avoidance

We first set up an R-SDS model in which a single male C57BL/6 mouse or a knockout mouse of the same genetic background (C57BL/6) was subjected to aggressive encounters with a male ICR mouse for 10 min daily, typically for 10 consecutive days (Figure 1A). To identify R-SDS-induced changes in gene expression profiles in the mPFC, we performed a transcriptome analysis in the mPFC without or with R-SDS. Because the level of social avoidance varies across individuals, we separately analyzed and compared the data from susceptible mice, which showed social avoidance after R-SDS, and resilient mice, which did not, in addition to those from naive mice, as reported previously

(E) The proportions of the time for the open arms in the elevated plus maze test as an index for anxiety of wild-type mice and TLR-DKO mice.

(F) The durations for the submissive posture during the first and tenth SDS (single and R-SDS, respectively) in wild-type mice and TLR-DKO mice.

* $p < 0.05$, ** $p < 0.01$, *** $p < 0.001$ for Bonferroni's multiple comparisons test. The number of mice is shown below each group. Data are shown as means \pm SEM. See also Figure S1.

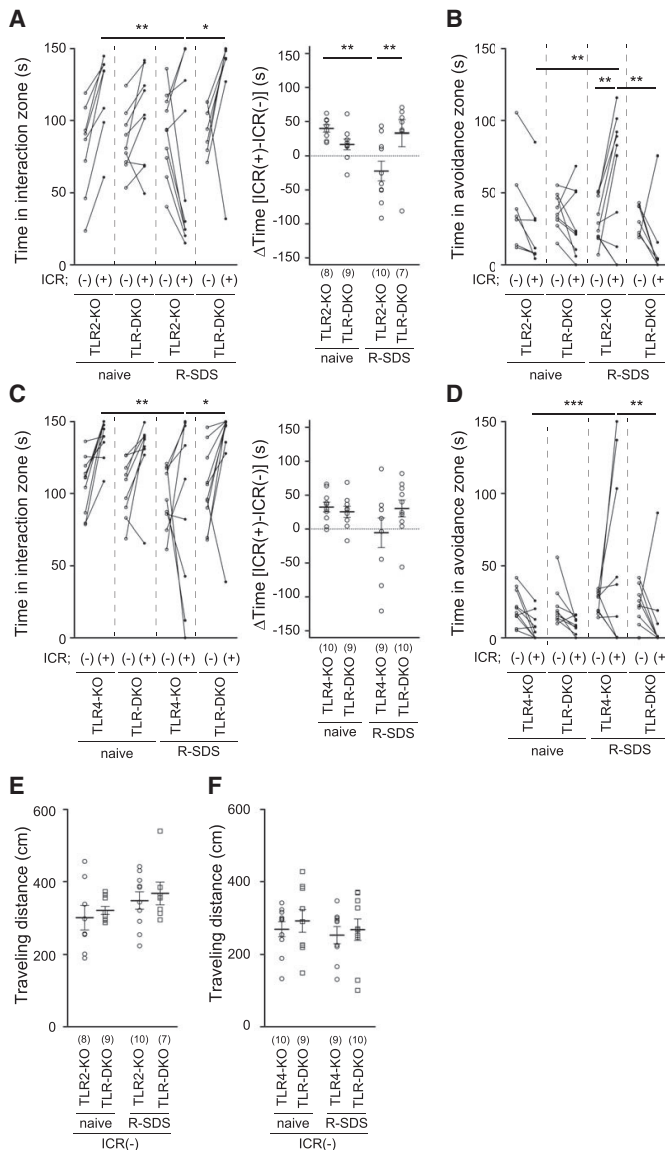


Figure 2. TLR2-KO Mice and TLR4-KO Mice, but Not TLR-DKO Littermates, Show R-SDS-Induced Social Avoidance

(A–D) The levels of social interaction (C) and social avoidance (D) in TLR2-KO and TLR-DKO littermates (A and B) or in TLR4-KO mice and TLR-DKO littermates (C and D) with or without prior R-SDS (R-SDS and naive, respectively). The data were analyzed and are shown as in Figures 1C and 1D.

(E and F) The traveling distances of TLR2-KO (E) and TLR4-KO mice (F) and TLR-DKO littermates in a novel open field with or without prior R-SDS.

* $p < 0.05$, ** $p < 0.01$, *** $p < 0.001$ for Bonferroni's multiple comparisons test. The number of mice is shown below each group. Data are shown as means \pm SEM. See also Figure S1.

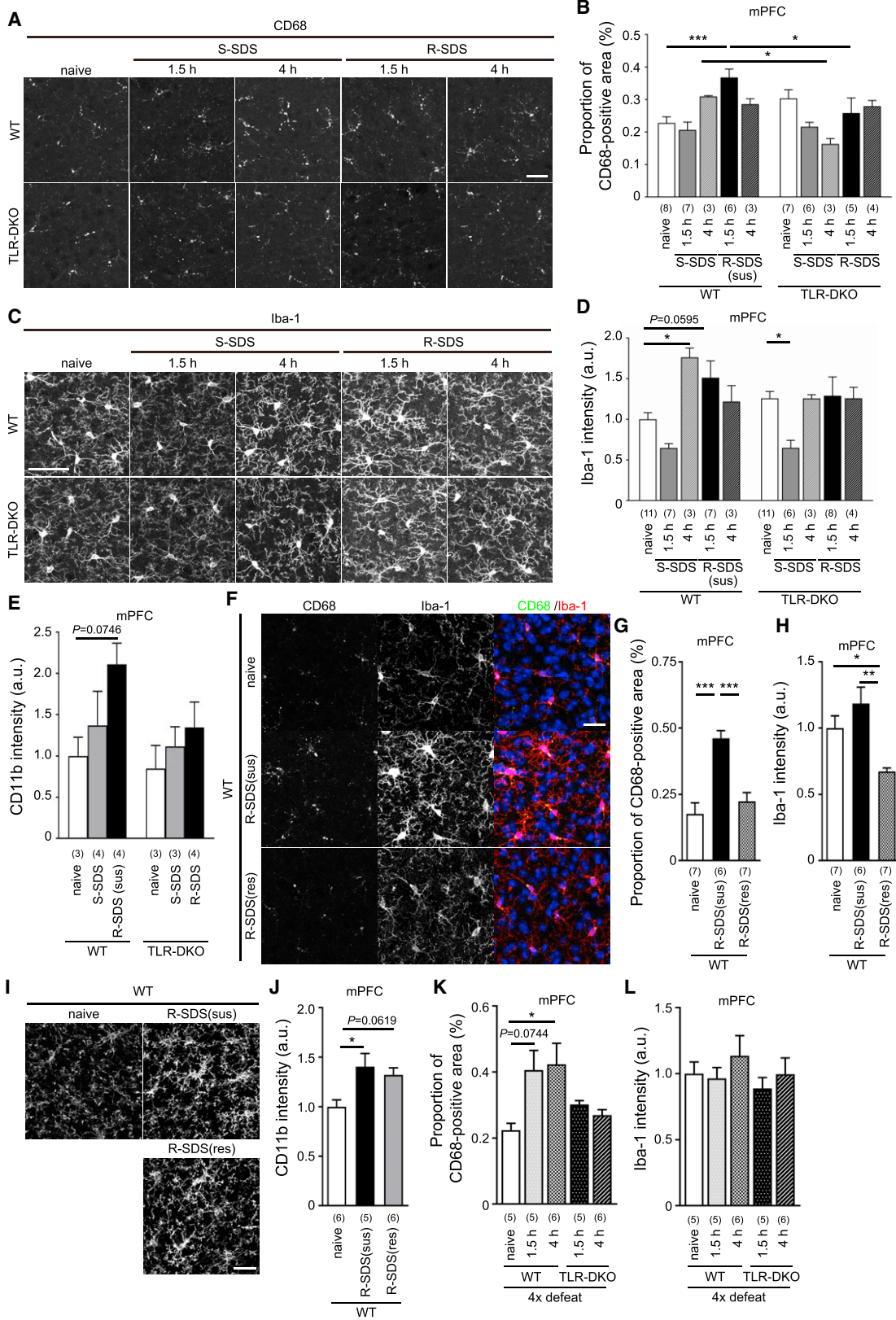
cytes (a minor population) in the EGFP-positive population was confirmed by mRNA expression of *Cd11b* (Integrin α M), a marker for microglia (Figure S1F). The expression levels of the *Tlr2* and *Tlr4* mRNAs were significantly higher in EGFP-positive cells, which include microglia, compared with those in EGFP-negative cells and were not affected by R-SDS (Figures S1G and S1H). On the other hand, the expression of mRNA for *Il1r1* (interleukin-1 [IL-1] receptor type I), which has been shown to be involved in stress-induced microglial changes in rodents (Kreisel et al., 2014), was detected only in EGFP-negative cells, and it was significantly upregulated by R-SDS (Figure S1I). These results demonstrate that microglia in the brain express TLR2 and TLR4 regardless of R-SDS.

We then examined whether TLR2/4 were involved in R-SDS-induced behavioral changes. In wild-type mice, R-SDS induced social avoidance in the social interaction test (i.e., decreased time for

the social interaction zone and increased time for the social avoidance zone; Figures 1B and 1C) and increased anxiety-like behavior in the elevated plus maze test (i.e., decreased time spent in open arms; Figure 1E), as reported previously (Tanaka et al., 2012). Mice lacking either *Tlr2* (TLR2 knockout [KO]) or *Tlr4* (TLR4-KO) also displayed R-SDS-induced social avoidance, as observed in wild-type mice (Figures 2A–2D, S1J, and S1K). Because TLR2 and TLR4 partly share an intracellular signaling pathway, we examined mice lacking *Tlr2* and *Tlr4* in combination (TLR double knockout [DKO]) and found that social avoidance was abolished in TLR-DKO mice (Figures 1C and 1D). Wild-type mice were categorized as either susceptible or resilient in a similar ratio (12 susceptible mice and 12 resilient mice), but TLR-DKO mice were mostly resilient (1 susceptible mouse and 18 resilient mice). The proportions of susceptible and resilient mice were significantly different between wild-type mice and

(Krishnan et al., 2007) (see the STAR Methods for the definitions of susceptible and resilient mice). This analysis revealed that R-SDS upregulates many inflammation-related genes in mPFC tissue, such as *S100a8*, *S100a9*, *Lipocalin2*, *Clec4d*, and *Ch25h* (cholesterol 25-hydroxylase) (Figures S1A–S1E). Among these genes, *S100a8* and *S100a9*, which were upregulated in both susceptible and resilient mice, have been shown to form a heterodimer, and, as ligands, to be functionally related to TLR4 and, possibly, TLR2 (Coveney et al., 2015; Vogl et al., 2007).

We then examined whether TLR2 and TLR4 were expressed in microglia before and after R-SDS. We subjected CX3CR1-EGFP mice, in which EGFP is selectively expressed in microglia in the brain and monocytes in peripheral tissues (Jung et al., 2000), to R-SDS and isolated EGFP-positive cells and EGFP-negative cells by fluorescence-activated cell sorting (FACS) from the whole brain of each mouse. Enrichment of microglia and mono-



(legend on next page)

TLR-DKO mice ($\chi^2 = 10.062$, $p = 0.0015$). In addition, TLR-DKO mice did not show elevated anxiety (Figure 1E). These results demonstrate that TLR2/4 are crucial for R-SDS-induced social avoidance and elevated anxiety. By contrast, wild-type mice and TLR-DKO mice similarly showed a submissive posture, a defensive posture induced by SDS (Tornatzky and Miczek, 1993), and its increase along the 10-day course of R-SDS (Figure 1F), suggesting that these mice are able to perceive R-SDS and to maintain its memory.

To exclude the potential effects of rearing conditions on phenotypes or to confirm the relationship between genotypes and phenotypes, we examined TLR-DKO mice and their littermates. Among the littermates obtained by crossing among TLR2-KO, TLR4-heterozygous mice (*Tlr2^{-/-};Tlr4^{+/+}*), TLR2-KO mice (*Tlr2^{-/-};Tlr4^{+/+}*), but not TLR-DKO littermates (*Tlr2^{-/-}; Tlr4^{-/-}*), showed R-SDS-induced social avoidance (Figures 2A and 2B). R-SDS-induced social avoidance was significantly suppressed in TLR-DKO littermates compared with TLR2-KO mice. Consistently, TLR2-KO mice were categorized as susceptible and resilient mice in a similar ratio (3 susceptible mice and 4 resilient mice), but none of the TLR-DKO littermates were susceptible (0 susceptible mice and 6 resilient mice). Likewise, social avoidance was intact in TLR4-KO mice (*Tlr2^{+/+};Tlr4^{-/-}*) but not in TLR-DKO littermates obtained by crossing among TLR2 heterozygous, TLR4-KO mice (*Tlr2^{+/+};Tlr4^{-/-}*) (Figures 2C and 2D). R-SDS-induced social avoidance was significantly suppressed in TLR-DKO littermates compared with TLR4-KO mice. Consistently, TLR4-KO mice were categorized as susceptible and resilient mice in a similar ratio (3 susceptible mice and 5 resilient mice), but none of the TLR-DKO littermates were susceptible (0 susceptible mice and 9 resilient mice). These results clearly demonstrate that the behavioral abnormalities of TLR-DKO mice are due to genotypes but not due to differences in rearing conditions. These abnormalities were not due to their locomotor deficits either; TLR-DKO mice showed locomotor activities similar to those of TLR2-KO or TLR4-KO littermates (Figures 2E and 2F).

We also analyzed *Il1r1* knockout (IL-1RI-KO) mice and found that R-SDS significantly induces social avoidance in IL-1RI-KO mice (Figures S1L and S1M). However, R-SDS-induced elevated anxiety was not apparent in these mice (Figure S1N), as reported previously (Wohleb et al., 2011). These results suggest that IL-1RI plays different roles than TLR2/4 in R-SDS-induced behavioral changes.

TLR2/4 Are Crucial for R-SDS-Induced Activation of mPFC Microglia in Susceptible Mice

Previous reports have shown involvement of the mPFC and NAc in repeated environmental stress-induced behavioral changes (Duman and Aghajanian, 2012; Krishnan and Nestler, 2008; McEwen and Morrison, 2013). We examined whether R-SDS as well as single social defeat stress (S-SDS) induced microglial activation in the mPFC and NAc and whether TLR2 and TLR4 were involved in these microglial responses. We performed immunostaining for several markers for microglial activation; namely, CD68, Iba-1, and CD11b (Hinwood et al., 2012). Among these markers, we first examined CD68, which showed the lowest signals under basal conditions without R-SDS. In wild-type mice, S-SDS appeared to increase the punctate area positive for CD68 signals in mPFC microglia 4 hr after S-SDS, whereas it did not change 1.5 hr after S-SDS (Figures 3A and 3B and S3A). By contrast, R-SDS increased the CD68-positive area in mPFC microglia 1.5 hr after the last session of R-SDS in susceptible wild-type mice (Figures 3A, 3B, 3F, and 3G), and this increase returned to the baseline 4 hr after R-SDS (Figures 3A and 3B). Indeed, the proportion of mice with the CD68-positive area beyond its distribution in naive mice was significantly larger in the total of defeated wild-type mice (including both susceptible and resilient mice) than in the total of TLR-DKO mice (14 of 19 and 4 of 13, respectively; $\chi^2 = 5.776$, $p = 0.016$; the wild-type and TLR-DKO mice used for this χ^2 analysis included all mice used for CD68 immunostaining in this study). We then examined Iba-1 signals in mPFC microglia. S-SDS appeared to decrease Iba-1 fluorescence intensity 1.5 hr but increased it 4 hr after S-SDS (Figures 3C and 3D). R-SDS appeared to increase Iba-1 fluorescence intensity 1.5 hr after the last exposure of R-SDS in susceptible wild-type mice, and this increase returned to the baseline 4 hr after R-SDS (Figures 3C and 3D). These findings demonstrate that R-SDS induces activation of mPFC microglia 4 hr after the last exposure to R-SDS and that SDS-induced activation of mPFC microglia occurs more rapidly with R-SDS, suggesting R-SDS-induced priming of mPFC microglia. Notably, both Iba-1 fluorescence intensity and the CD68-positive area in mPFC microglia after R-SDS were significantly higher in susceptible wild-type mice than in resilient wild-type mice (Figures 3F–3H), indicating that R-SDS-induced activation of mPFC microglia is correlated with the level of social avoidance.

Figure 3. TLR2/4 Are Crucial for R-SDS-Induced Activation of mPFC Microglia

(A–D) Representative images (A and C) and quantitative analyses (B and D) of CD68 (A and B) and Iba-1 (C and D) immunostaining in the mPFC of wild-type mice and TLR-DKO mice without SDS (naive) and 1.5 hr and 4 hr after S-SDS and the last session of R-SDS. For wild-type mice after R-SDS, the images were taken and analyzed only from susceptible mice (R-SDS(sus)). Scale bars, 50 μ m.

(E) Quantitative analyses of CD11b immunostaining in the mPFC of wild-type mice and TLR-DKO mice without SDS (naive) and 1.5 hr after S-SDS and the last session of R-SDS. For wild-type mice after R-SDS, the images were taken and analyzed only from susceptible mice (R-SDS(sus)).

(F–J) Representative images (F and I) and quantitative analyses (G, H, and J) of immunostaining for CD68 and Iba-1 (F–H) or CD11b (I and J) in the mPFC of wild-type mice without SDS (naive) and susceptible and resilient mice 1.5 h after the last session of R-SDS (R-SDS(sus) and R-SDS(res), respectively). In the merged images in (F), CD68 and Iba-1 signals are shown in green and red, respectively. CD68 signals in Iba-1-positive microglia are shown in yellow. Nuclei were counterstained with Hoechst33342 and are shown in blue. Scale bars, 25 μ m.

(K and L) Quantitative analyses of CD68 (K) and Iba-1 (L) immunostaining in the mPFC of wild-type mice and TLR-DKO mice without SDS (naive) and 1.5 hr and 4 hr after the last session of R-SDS for 4 days (4 \times defeat).

* $p < 0.05$, ** $p < 0.01$, *** $p < 0.001$ for Bonferroni's multiple comparison test. The values of Iba-1 and CD11b intensity were normalized to those of naive wild-type mice. The number of mice is shown below each group. Data are shown as means \pm SEM. See also Figures S2 and S3.

We also found that R-SDS increases CD11b signals in mPFC microglia 1.5 hr after the last exposure of R-SDS but not after S-SDS (Figures 3E, 3I, and 3J) in both susceptible and resilient wild-type mice (Figures 3I and 3J). Our statistical analysis also indicated that CD68 signals in the mPFC after R-SDS are more strongly correlated with the level of social avoidance than Iba-1 signals (CD68: $r^2 = 0.6977$, $p < 0.0001$; Iba-1: $r^2 = 0.3387$, $p = 0.0142$ for the time in the avoidance zone) Thus, among the three conventional markers for microglial activation, R-SDS-induced increases in CD68 signals in mPFC microglia were most strongly correlated with the level of social avoidance.

Because we previously showed that R-SDS for 4 days was sufficient to induce social avoidance (Tanaka et al., 2012), we also performed immunostaining for CD68 and Iba-1 1.5 hr and 4 hr after R-SDS for 4 days. R-SDS for 4 days increased CD68-positive areas in mPFC microglia at both of these time points (Figure 3K). Although Iba-1 intensity did not appear to increase after R-SDS for 4 days (Figure 3L), Iba-1 decrease, which occurred 1.5 hr after S-SDS (Figure 3D), was not observed 1.5 hr after R-SDS for 4 days (Figure 3L). These results indicated that R-SDS for 4 days induces an intermediate pattern of microglial activation between those induced by S-SDS and R-SDS for 10 days.

We then examined whether TLR2/4 deficiency affected R-SDS-induced activation of mPFC microglia. In TLR-DKO mice, S-SDS did not increase the CD68-positive area in mPFC microglia (Figures 3A and 3B). The CD68-positive area 4 hr after S-SDS was significantly smaller in TLR-DKO mice than in susceptible wild-type mice. The S-SDS-induced increase in Iba-1 fluorescence intensity in the mPFC 4 hr after S-SDS was also abolished in TLR-DKO mice (Figures 3C and 3D). These results indicated that TLR2/4 are crucial for S-SDS-induced activation of mPFC microglia. By contrast, 1.5 hr after S-SDS, Iba-1 signals were decreased in TLR-DKO mice, as similarly observed in wild-type mice, indicating that this microglial response was not mediated by either TLR2 or TLR4. In addition, TLR-DKO mice did not show an R-SDS-induced increase in CD68 signals in mPFC microglia 1.5 h after the last exposure of R-SDS, which was observed in susceptible wild-type mice (Figures 3A and 3B). These results demonstrate that TLR2/4 are crucial for the activation of mPFC microglia induced by R-SDS as well as that induced by S-SDS. Note that neither the fluorescence intensity of Iba-1 signals nor that of CD11b was affected by R-SDS in TLR-DKO mice (Figures 3C–3E). It was also noted that neither TLR2 nor TLR4 deficiency affected the signals of CD68, Iba-1, or CD11b under the basal condition without SDS (Figures 3A–3E and S2A–S2F).

We also examined the roles of TLR2/4 in R-SDS-induced microglial activation in TLR-DKO littermates obtained from the heterozygous crossing. The R-SDS-induced CD68 increase in mPFC microglia was abolished in TLR-DKO littermates, although it remained in susceptible mice with the TLR4-KO genotype (Figures S2A, S2B, S2D, and S2E). Iba-1 fluorescence intensity was not significantly increased in any of these genotypes (Figures S2A, S2C, S2D, and S2F). These results suggest that the respective markers for microglial activation may be differently regulated. Neither TLR2/4 deficiency nor R-SDS affected the number of Iba-1-positive microglia in the mPFC (data not shown). These results demonstrate that the lack of R-SDS-induced activation of

mPFC microglia in TLR-DKO mice is due to the TLR2/4 deletion but not due to differences in rearing conditions. By contrast, neither S-SDS nor R-SDS significantly increased Iba-1 or CD68 signals in NAc microglia of either wild-type mice or TLR-DKO mice (Figures S3B–S3G).

As reported previously (Wohleb et al., 2013), R-SDS promotes infiltration of CD45-positive monocytes to the anterior cingulate cortex (ACC), which is located dorsal to the mPFC, in susceptible wild-type mice (Figures 4A, 4C, 4E, and 4G). However, this monocyte infiltration in the ACC was unaffected in TLR-DKO mice. Notably, monocyte infiltration did not occur in the mPFC, in which R-SDS induces microglial activation (Figure 3), in either wild-type or TLR-DKO mice (Figures 4B, 4D, and 4F). Thus, R-SDS induces microglial activation in the mPFC and monocyte infiltration in the ACC, and TLR2/4 are involved in the former but not in the latter.

TLR2/4 Are Crucial for the Attenuation of SDS-Induced c-Fos Expression and Dendritic Atrophy of mPFC Neurons by R-SDS in Susceptible Mice

We next examined whether TLR2/4 are involved in SDS-induced neuronal responses in the mPFC using immunostaining for c-Fos, a marker for neuronal response (Figure 5A). S-SDS induced c-Fos expression in mPFC neurons of both wild-type and TLR-DKO mice (Figures 5B and 5C). This c-Fos expression was abolished by R-SDS in susceptible wild-type mice but maintained in resilient wild-type mice (Figures 5D and 5E). In TLR-DKO mice, R-SDS attenuated SDS-induced c-Fos expression, but it was maintained at a level similar to resilient wild-type mice (approximately 25 neurons/mm² in both mice) (Figures 5B–5E). Indeed, the proportion of mice with a number of c-Fos-positive cells beyond its distribution in naive mice was significantly smaller in the total of defeated wild-type mice (including both susceptible and resilient mice) than in the total of defeated TLR-DKO mice (12 of 18 and 16 of 17, respectively; $\chi^2 = 4.118$, $p = 0.042$; the wild-type and TLR-DKO mice used for this χ^2 analysis included all mice used for c-Fos immunostaining in this study). These findings were confirmed with littermates obtained by crossing among TLR2-heterozygous, TLR4-KO mice or TLR2-KO, TLR4-heterozygous mice. SDS-induced c-Fos expression was observed in resilient but not susceptible mice with the TLR2-KO or TLR4-KO genotype (Figure S4), as observed in wild-type mice. In TLR-DKO littermates, this SDS-induced c-Fos expression was maintained, as observed in resilient TLR2-KO or TLR4-KO mice. These results indicate that TLR2/4 are involved in the attenuation of SDS-induced c-Fos expression in mPFC neurons by R-SDS in susceptible mice.

Repeated environmental stress induces dendritic atrophy of mPFC neurons, which is thought to underlie concomitant behavioral changes (Duman and Aghajanian, 2012; McEwen and Morrison, 2013). We performed Golgi-Cox staining and measured the lengths of apical dendrites of mPFC deep-layer pyramidal neurons. R-SDS induced shortening of apical dendrites of mPFC neurons in susceptible wild-type mice, whereas TLR-DKO mice did not show this dendritic shortening (Figures 5F–5H). These results indicate that TLR2/4 are crucial for dendritic atrophy of mPFC neurons induced by R-SDS in susceptible mice.

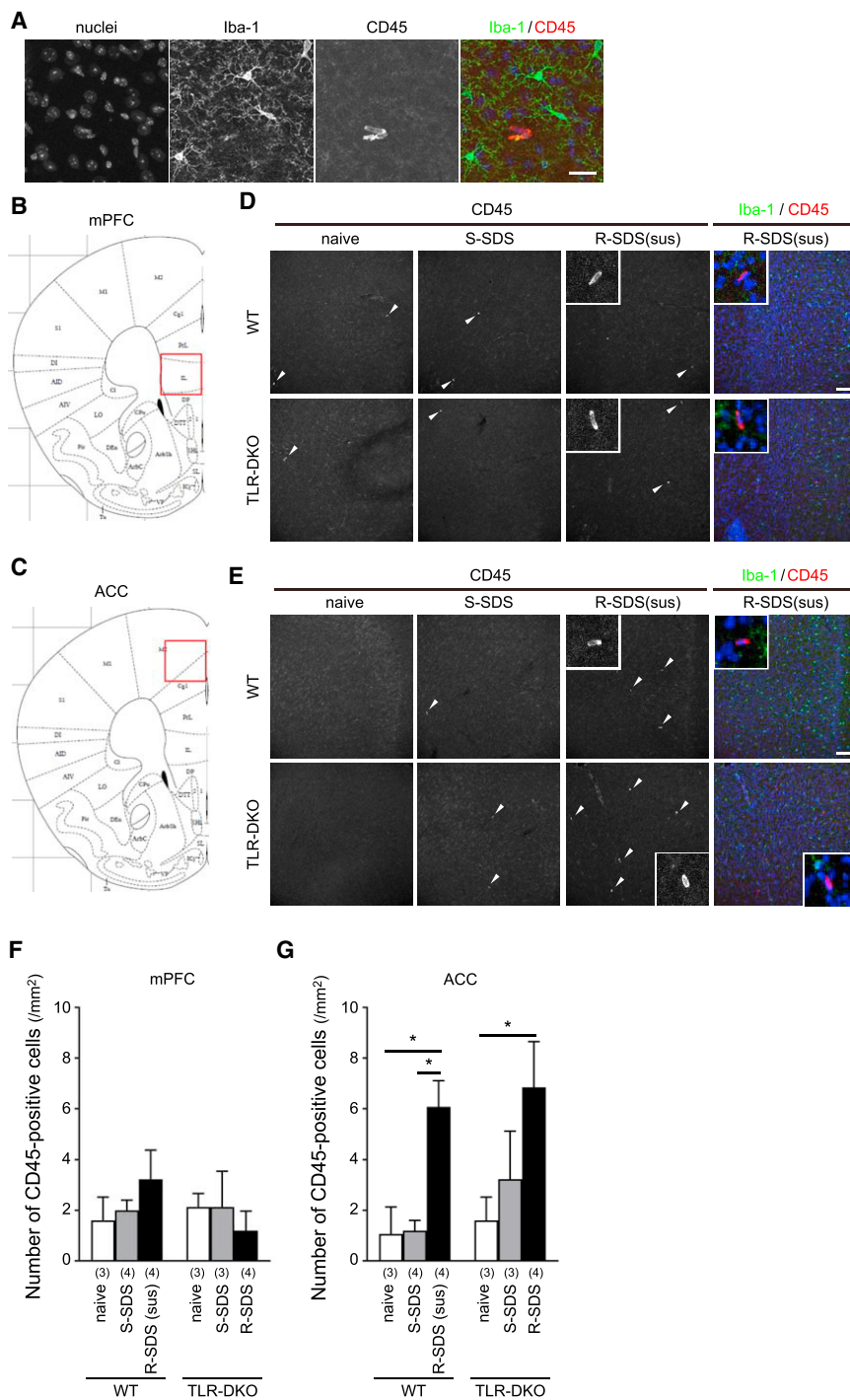


Figure 4. R-SDS Promotes Monocyte Infiltration into the ACC, but Not the mPFC, in a TLR2/4-Independent Manner

(A) Representative images of CD45-positive monocytes in the mPFC. Microglia were visualized by Iba-1 staining. Nuclei were counterstained with Hoechst 33342. In the merged image, signals for Iba-1, CD45, and Hoechst33342 are shown in green, red, and blue, respectively. Scale bar, 25 μm.

(B and C) Regions of interest in the mPFC (B) and ACC (C).

(D–G) Representative images (D and E) and quantitative analyses (F and G) of CD45 immunostaining in the mPFC (D and F) and ACC (E and G) of wild-type mice and TLR-DKO mice without SDS (naive) and 1.5 hr after S-SDS and the last session of R-SDS. Iba-1 and CD45 immunostaining and nuclear counterstaining with Hoechst33342 were performed as described in (A). For wild-type mice after R-SDS, the images were taken and analyzed only from susceptible mice (R-SDS(sus)). Arrowheads in (D) and (E) indicate the representative CD45⁺ cells. Scale bars, 100 μm.

*p < 0.05 for Bonferroni's multiple comparison test. The number of mice is shown below each group. Data are shown as means ± SEM.

derived from wild-type neonates to the spinal cord has been used to investigate the roles of microglia in neuropathic pain (Tsuda et al., 2003). We examined whether transplantation of these cells into the mPFC of TLR-DKO mice could restore R-SDS-induced social avoidance (Figure S5A). One week after the transplantation, microglia-like cells labeled with carboxyfluorescein succinimidyl ester (CFSE), a semi-permanent fluorescent tracer, showed an ameboid morphology reminiscent of maximally activated microglia (data not shown). After a 4-week recovery period, these cells remained around the injection site and appeared to show a ramified morphology, suggesting that the transplanted microglia had become inactive (Figure S5B). Transplantation of wild-type, but not TLR-DKO, microglia-like cells to the mPFC of TLR-DKO mice significantly restored social avoidance induced by R-SDS for

4 days (Figures S5D–S5G). Without R-SDS, the transplantation of these microglia-like cells did not induce social avoidance in TLR-DKO mice (Figures S5E and S5G). These findings indicate that the transplantation of wild-type microglia-like cells to the mPFC restores the induction of social avoidance in a TLR2/4-dependent manner. However, this restoration was not sustained after R-SDS for 10 days (Figures S5H–S5K), although

TLR2/4 in mPFC Microglia Are Crucial for R-SDS-Induced Social Avoidance

Because TLR2/4 are highly expressed in microglia (Figures S1G and S1H) and required for R-SDS-induced activation of mPFC microglia, as described above, we examined whether mPFC microglia are important for R-SDS-induced social avoidance. Transplantation of cultured microglia-like cells

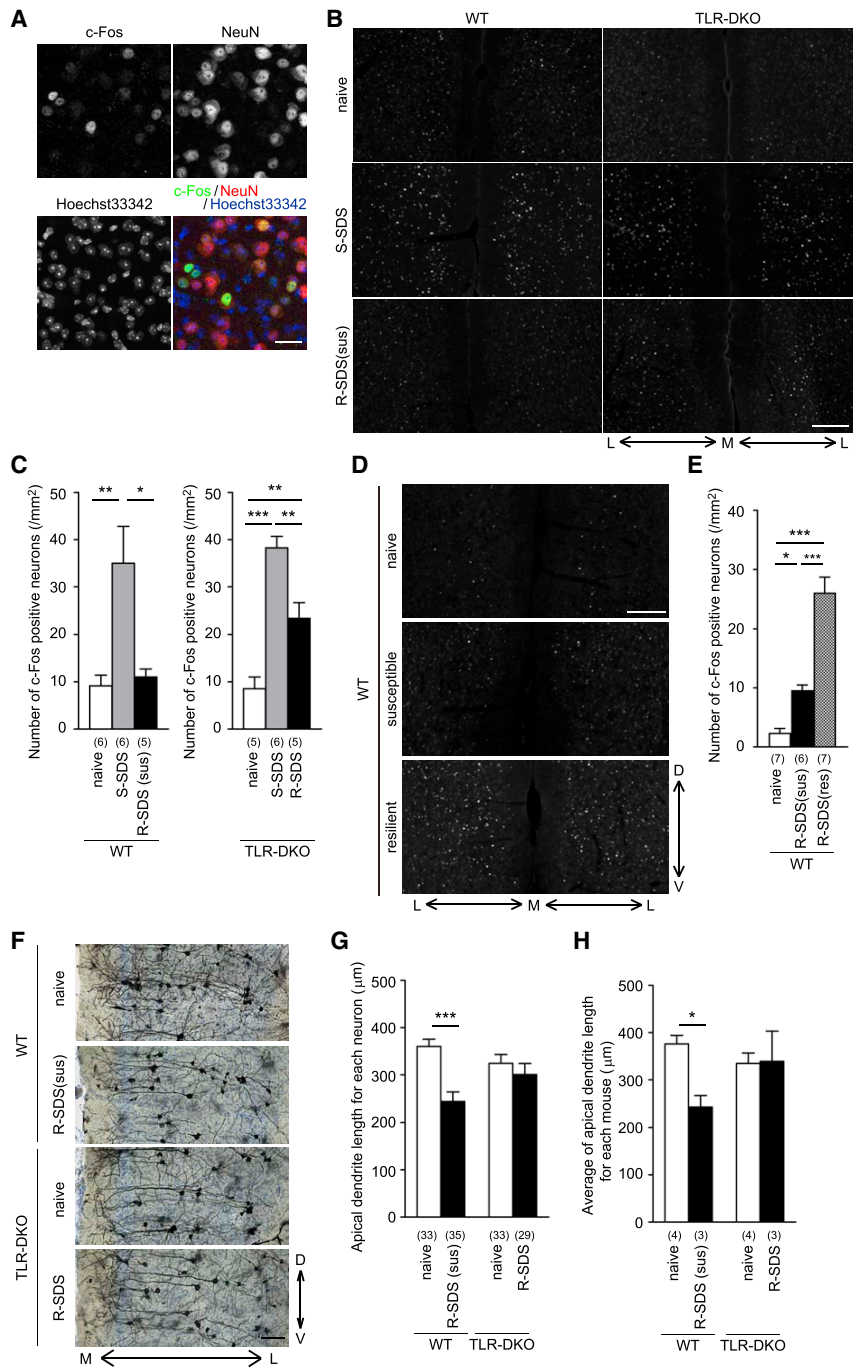


Figure 5. TLR2/4 Are Required for the Attenuation of SDS-Induced c-Fos Expression and Dendritic Atrophy of mPFC Neurons by R-SDS

(A) Representative images of double immunostaining of c-Fos and NeuN, a neuronal marker, in the mPFC. Nuclei were counterstained with Hoechst33342. In the merged image, signals for c-Fos, NeuN, and Hoechst33342 are shown in green, red, and blue, respectively. Scale bar, 25 μ m. (B and C) Representative images (B) and quantitative analyses (C) of c-Fos immunostaining in the mPFC of wild-type mice and TLR-DKO mice without SDS (naive) and 1.5 hr after S-SDS and R-SDS. For wild-type mice after R-SDS, the image was taken from susceptible mice (R-SDS(sus)). Scale bar, 200 μ m.

(D and E) Representative images (D) and quantitative analyses (E) of c-Fos immunostaining in the mPFC of wild-type mice without SDS (naive) and susceptible mice and resilient mice 1.5 hr after the last session of R-SDS (R-SDS(sus)) and R-SDS(res), respectively. Scale bar, 200 μ m.

(F–H) Representative images of Golgi-Cox staining in the mPFC (F) and quantitative analyses of the lengths of apical dendrites of mPFC deep-layer pyramidal neurons (G and H) of wild-type mice and TLR-DKO mice with or without R-SDS (R-SDS or naive, respectively). Brain sections were counterstained with cresyl violet. For wild-type mice after R-SDS, the images were taken and analyzed only from susceptible mice (R-SDS(sus)). Scale bar, 100 μ m.

* $p < 0.05$, ** $p < 0.01$, *** $p < 0.001$ for Bonferroni's multiple comparisons test. The orientations of the images (B–F) are indicated by arrows (L, lateral; M, medial; D, dorsal; V, ventral). The number of mice (C, E, and H) or neurons (G) is shown below each group. Data are shown as means \pm SEM. See also Figure S4.

the transplanted cells were maintained similarly among the comparison groups (Figure S5C).

To examine whether TLR2/4 in mPFC microglia are necessary for R-SDS-induced behavioral changes, we developed a method to reduce TLR2/4 expression specifically in mPFC microglia. For this purpose, we generated a lentiviral vector expressing artificial microRNAs targeting *Tlr2* and *Tlr4* mRNAs only in cells expressing Cre recombinase driven by the microglial-specific CX3CR1 promoter (Figure 6A). The specificity and efficiency of *Tlr2* and

Tlr4 microRNAs were validated in Lenti-X 293T cells overexpressing the respective TLR isoforms together with *Tlr2* or *Tlr4* microRNA (Figure S6A). Expression of *Tlr2* or *Tlr4* microRNA efficiently reduced the mRNA level of the corresponding *Tlr* isoform by approximately 80%, but not those of the other TLR isoforms, confirming the specificity of the *Tlr2* or *Tlr4* microRNAs (Figure S6A). In addition, in the N9 microglial cell line, lentivirus-delivered tandem-connected *Tlr2* or *Tlr4* microRNAs (TLR2/4 microRNA) reduced endogenous expression of both *Tlr2* or *Tlr4* (reduction by ~40% and ~60%, respectively) (Figure S6B).

Each lentiviral vector, which is able to express TLR2/4 microRNA or control microRNA only in cells expressing Cre recombinase, was injected into the mPFC of CX3CR1-CreER mice, in which tamoxifen-inducible Cre recombinase and enhanced yellow fluorescent protein (EYFP) are selectively expressed in microglia (Parkhurst et al., 2013). Four weeks after

the lentiviral injection and tamoxifen treatment (Figure 6B), many EYFP-positive cells, mostly microglia, showed mCherry signals that were designed to co-express TLR2/4 or control microRNAs (Figures 6C, 6D, and 6F). Most mCherry signals were observed in EYFP-positive cells, but much less in CD45-positive monocytes, without or with R-SDS (Figures 6E–6G), suggesting that the mice were specifically expressing TLR2/4 or control microRNAs in mPFC microglia. Expression of TLR2/4 microRNAs in mPFC microglia by this method abolished R-SDS-induced social avoidance, whereas this social avoidance was induced in mice that had received the lentiviral vector expressing control microRNA (Figures 6H and 6I). To exclude off-target effects of these microRNAs, we generated microRNA-resistant synonymous mutant cDNAs of *Tlr2* or *Tlr4* (i.e., without changing their amino acid sequences) and confirmed that the protein expression levels of these mutants were resistant to the respective microRNAs in Lenti-X 293T cells (Figures S6C–S6H). We generated lentiviral vectors expressing either of these mutants along with TLR2/4 microRNA in the presence of Cre recombinase and injected these lentiviral vectors into the mPFC of CX3CR1-CreER mice. Simultaneous expression of the microRNA-resistant *Tlr2* or *Tlr4* mutant restored R-SDS-induced social avoidance in the presence of TLR2/4 microRNA (Figures 6J and 6K). These results excluded off-target effects of TLR2/4 microRNA and demonstrated that TLR2/4 in mPFC microglia are crucial for R-SDS-induced social avoidance. By contrast, mPFC microglia-specific expression of TLR2/4 microRNA did not appear to affect R-SDS-induced elevated anxiety (Figure 6L).

We also examined the effect of TLR2/4 microRNA in mPFC microglia on SDS-induced c-Fos expression in mPFC neurons. The number of c-Fos-positive mPFC neurons in mice expressing TLR2/4 microRNA in mPFC microglia was significantly larger compared with susceptible mice without TLR2/4 microRNA expression (Figure 6M). Consistent with the experiments using TLR-DKO mice, these results indicate that TLR2/4 in mPFC microglia are involved in the attenuation of SDS-induced c-Fos expression in mPFC neurons by R-SDS in susceptible mice.

In addition, we evaluated the effect of TLR2/4 microRNA on excitatory synapses in mPFC neurons using super-resolution structured illumination microscopy (SIM) (Figure S7A). Surprisingly, R-SDS significantly increased the number of punctate signals of PSD95, a postsynaptic marker, in the deep layer of the mPFC in susceptible wild-type mice with expression of control microRNA in mPFC microglia. This effect was abolished by expression of TLR2/4 microRNA in mPFC microglia (Figure S7B). R-SDS appeared to increase the number of punctate signals of synaptophysin, a presynaptic marker, although this increase was milder and not statistically significant (Figure S7C). These results suggest that R-SDS increases the number of excitatory synapses in the mPFC in a manner dependent on TLR2/4 expressed in mPFC microglia.

IL-1 α and TNF- α Are Upregulated in mPFC Microglia by R-SDS in a TLR2/4-Dependent Manner and Are Crucial for R-SDS-Induced Social Avoidance

Based on our observations that R-SDS induces different microglial responses in the mPFC and NAc (Figures 3 and S3), we performed a transcriptome analysis of microglia isolated from the

mPFC or NAc without or with R-SDS (Figures 7A–7C). We found that different sets of genes are significantly up- or downregulated by R-SDS in microglia isolated from the two brain areas (Figures 7D and 7E). Among these genes, several cytokines, such as *Tnfa* and *Il1a*, were significantly upregulated in mPFC microglia, and marginally in NAc microglia, in a TLR2/4-dependent manner (Figures 7F–7I). In contrast, *Ccl3* and *Ccl4* appeared to be upregulated in both mPFC and NAc microglia in a TLR2/4-dependent manner (Figures 7F and 7G). Although *Il1b* and *Il6* also appeared to be upregulated in both mPFC and NAc microglia, the involvement of TLR2/4 was elusive (Figures 7F, 7G, 7J, and 7K).

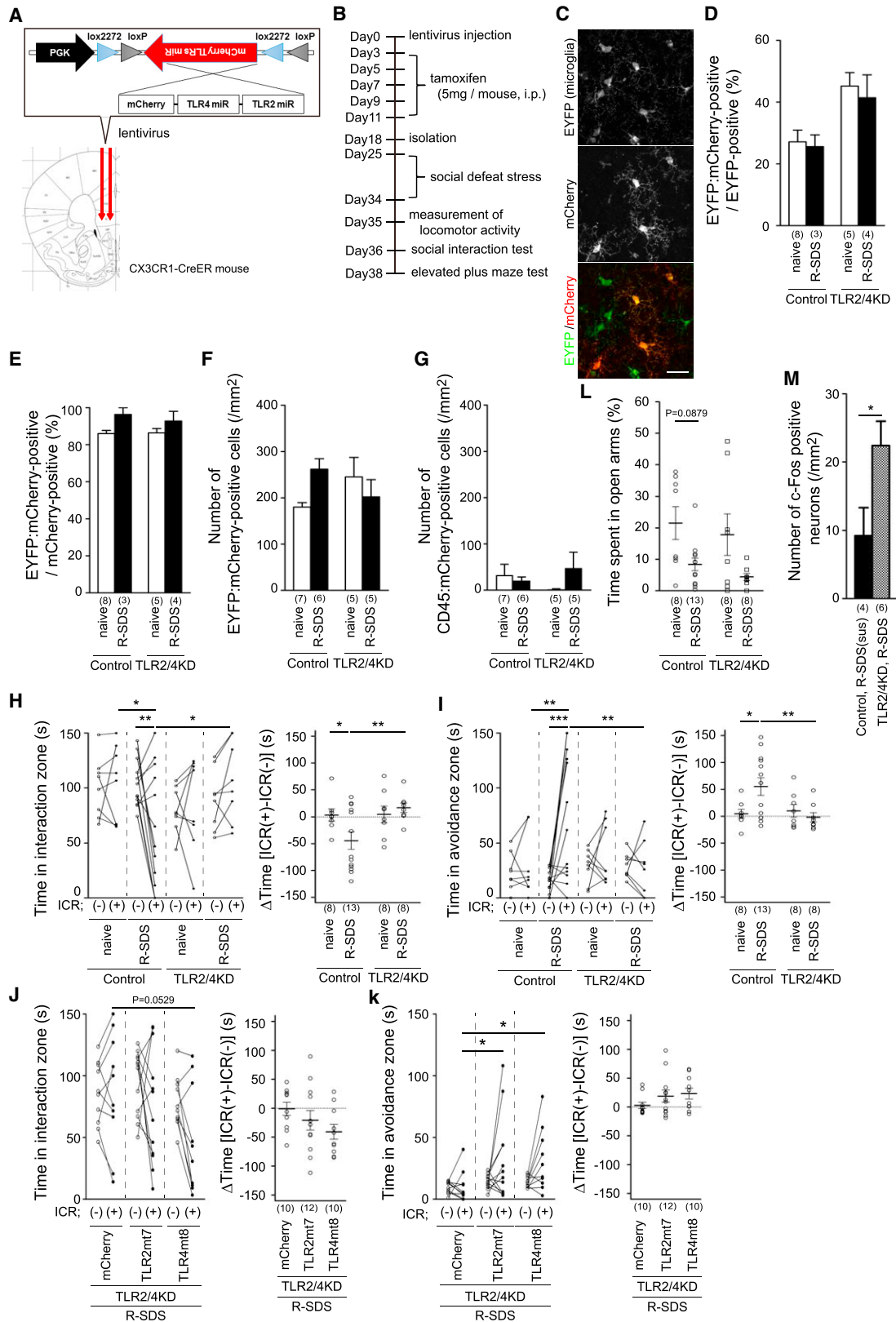
To examine whether IL-1 α and tumor necrosis factor alpha (TNF- α) in the mPFC are involved in R-SDS-induced social avoidance, we infused neutralizing antibodies for these cytokines into the mPFC. To reduce the amounts of the antibodies to be used, we employed a shorter version of R-SDS, which is composed of three exposures to SDS within a single day (Figure 8A). This shorter version of R-SDS appeared to increase CD68 signals in microglia in the mPFC, but not in the NAc, 1.5 hr and 4 hr after R-SDS (Figures S2G–S2J). We administered a mixture of neutralizing antibodies for IL-1 α and TNF- α into the mPFC 2 hr before R-SDS and found that the normal R-SDS-induced CD68 increase in mPFC microglia was absent with these neutralizing antibodies in the mPFC. Notably, this shorter version of R-SDS significantly decreased the time in the interaction zone, indicating induction of social avoidance, although it only moderately increased the time in the avoidance zone (Figures 8B and 8C), compared with the original longer version of R-SDS. mPFC infusion of these neutralizing antibodies abolished these behavioral changes. Either of these antibodies also blocked the induction of social avoidance (Figures 8D and 8E). These results strongly indicate that IL-1 α and TNF- α , associated with mPFC microglia activated by R-SDS, are responsible for the induction of social avoidance.

DISCUSSION

In this study, we found that TLR-DKO mice show resilience to R-SDS-induced social avoidance and anxiety. TLR2/4 are also crucial for R-SDS-induced activation of mPFC microglia as well as response attenuation and dendritic atrophy of mPFC neurons. These microglial activation and neuronal changes occur in susceptible but not resilient mice. Knockdown of TLR2/4 in mPFC microglia abolishes R-SDS-induced social avoidance. *Il1a* and *Tnfa* are upregulated in mPFC microglia by R-SDS in a manner dependent on TLR2/4 and are crucial for R-SDS-induced social avoidance. These findings link TLR2/4 function in mPFC microglia to neuronal and microglial changes in the mPFC, leading to R-SDS-induced social avoidance. In our model, R-SDS activates mPFC microglia through TLR2/4, which attenuates the stress response of mPFC neurons and induces social avoidance through IL-1 α and TNF- α (Figure S8).

TLR2/4 in mPFC Microglia Mediate R-SDS-Induced Social Avoidance

In this study, we showed that TLR2/4 mediate R-SDS-induced social avoidance and elevated anxiety as well as neuronal and



(legend on next page)

microglial changes in the mPFC. Our transcriptome analysis demonstrated that R-SDS increases the mRNA levels of *S100a8* and *S100a9*, potential ligands for TLR2/4, in the mPFC of susceptible and resilient mice. It remains to be examined whether the S100A8/S100A9 heterodimer is released into the extracellular space in response to R-SDS and acts as an endogenous TLR2/4 ligand for R-SDS-induced activation of mPFC microglia. Notably, our histological examinations showed that R-SDS induces microglial activation in susceptible but not resilient mice. Thus, *bona fide* TLR ligands other than S100A8/S100A9 could be upregulated and/or secreted specifically in the mPFC.

Previous studies have reported roles of several molecules in repeated environmental stress-induced microglial activation, but none of these studies identified their sites of action. Although it is difficult to manipulate gene expression selectively in microglia in a given brain area, transplantation of microglia-like cells obtained from neonates has been used to elucidate the roles of microglia in the spinal cord in neuropathic pain (Tsuda et al., 2003). We used similar transplantation methods in the brain and found that wild-type, but not TLR-DKO, microglia-like cells transplanted into the mPFC of TLR-DKO mice restored R-SDS-induced social avoidance. However, the effect of this transplantation was transient, and recent studies have revealed differences in gene expression profiles between microglia *in vitro* and *in vivo* and between neonatal and adult microglia (Butovsky et al., 2014). Therefore, we developed a lentivirus-based method to express TLR2/4 microRNA selectively in mPFC microglia. Using this method, most cells expressing TLR2/4 or control microRNA were microglia rather than infiltrated monocytes in the mPFC, and selective TLR2/4 knockdown in mPFC microglia abolished R-SDS-induced social avoidance. These results document, for the first time, the critical roles of innate immune receptors in microglia in repeated environmental stress-induced behavioral changes and provide the first evidence for mPFC microglia as the site of action of molecules involved in repeated environmental stress-induced microglial activation.

However, we note that our findings did not exclude the possibility that TLR2/4 in non-microglial cells or in other brain areas may also be involved in behavioral changes. Indeed, we found that systemic TLR2/4 deficiency, but not specific TLR2/4 knockdown in mPFC microglia, abolishes R-SDS-induced elevated anxiety. In addition, other brain areas, such as the ventral hippo-

campus and amygdala, have been shown to be involved in R-SDS-induced behavioral changes (Bagot et al., 2015; Wohleb et al., 2011).

Many rodent studies have suggested a role of IL-1 β in anhedonia after chronic unpredictable stress and elevated anxiety induced by R-SDS (Goshen et al., 2008; Koo and Duman, 2008; Wohleb et al., 2011). It has recently been reported that mice lacking NLRP3, a component of the inflammasome that converts pro-IL-1 β to its active form, show decreased anxiety without stress and lack of anhedonia after chronic unpredictable stress (Iwata et al., 2015). However, we observed that the IL-1RI deletion did not abolish R-SDS-induced social avoidance and that *Tlr2* and *Tlr4*, but not *Il1r1*, are expressed in microglia. These different expressions may explain why TLR2/4, rather than IL-1RI, are integral to social avoidance. It has been reported that IL-1RI is critical for R-SDS-induced monocyte infiltration and elevated anxiety (Wohleb et al., 2013) and that splenectomy prevents an anxiety tendency induced by R-SDS (McKim et al., 2016). Thus, IL-1RI-mediated monocyte infiltration has been proposed to be involved in R-SDS-induced elevated anxiety. By contrast, TLR2/4 deficiency did not affect monocyte infiltration from the periphery to the ACC, and IL-1RI deficiency did not affect R-SDS-induced social avoidance. These findings indicate that different inflammation-related mechanisms underlie R-SDS-induced social avoidance and elevated anxiety.

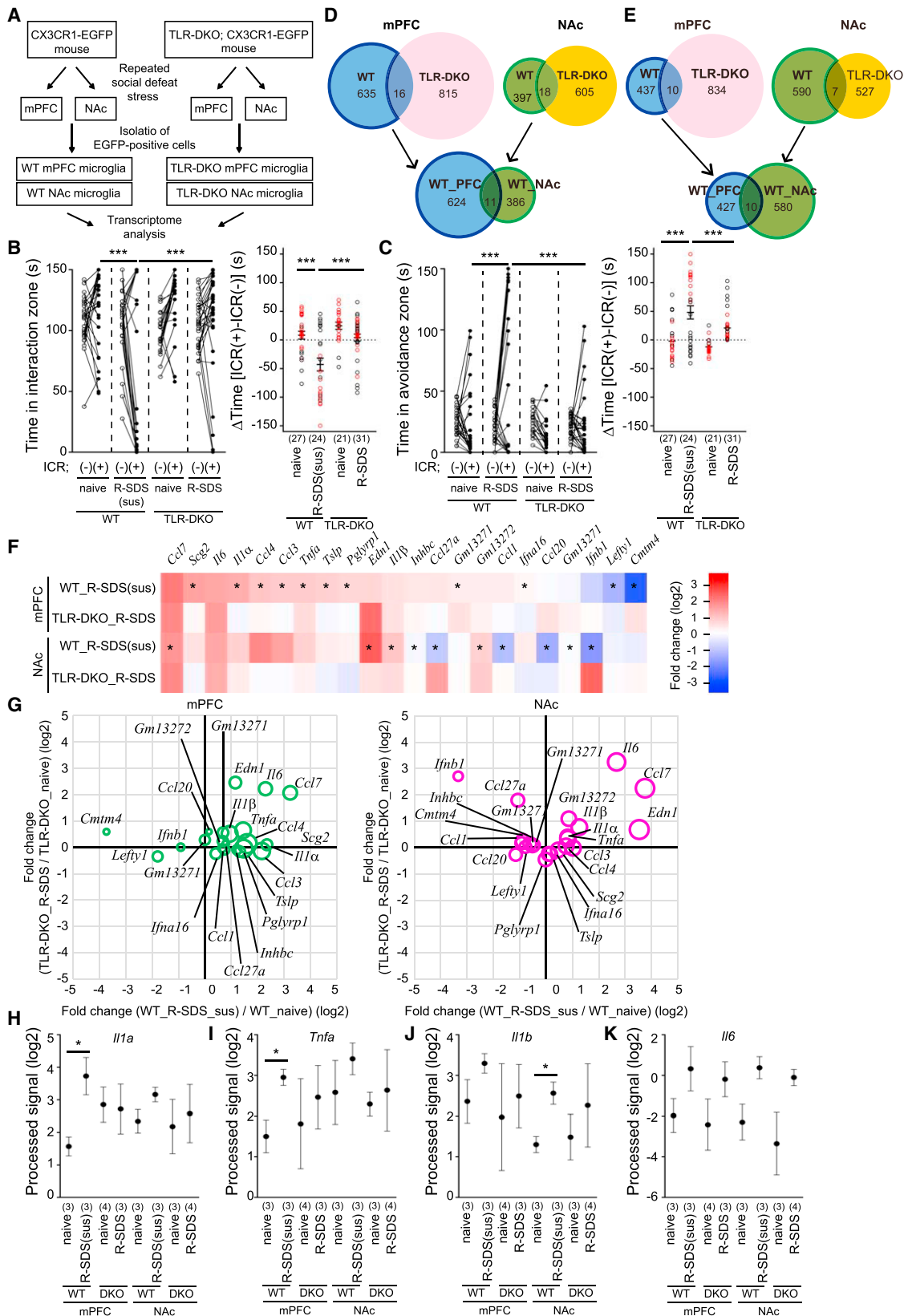
TLR2/4 in Microglia Mediate R-SDS-Induced Neuronal Remodeling in the mPFC

Based on our observation that TLR2/4 in mPFC microglia are crucial for R-SDS-induced social avoidance, we speculated that R-SDS-activated mPFC microglia could locally affect mPFC neurons. Indeed, we showed that systemic TLR2/4 deletion mitigates R-SDS-induced c-Fos response attenuation and dendritic atrophy in mPFC neurons and that mPFC microglia-specific TLR2/4 knockdown at least mitigates the former of these R-SDS-induced changes. These findings indicate that TLR2/4 in mPFC microglia are involved in R-SDS-induced changes in mPFC neurons.

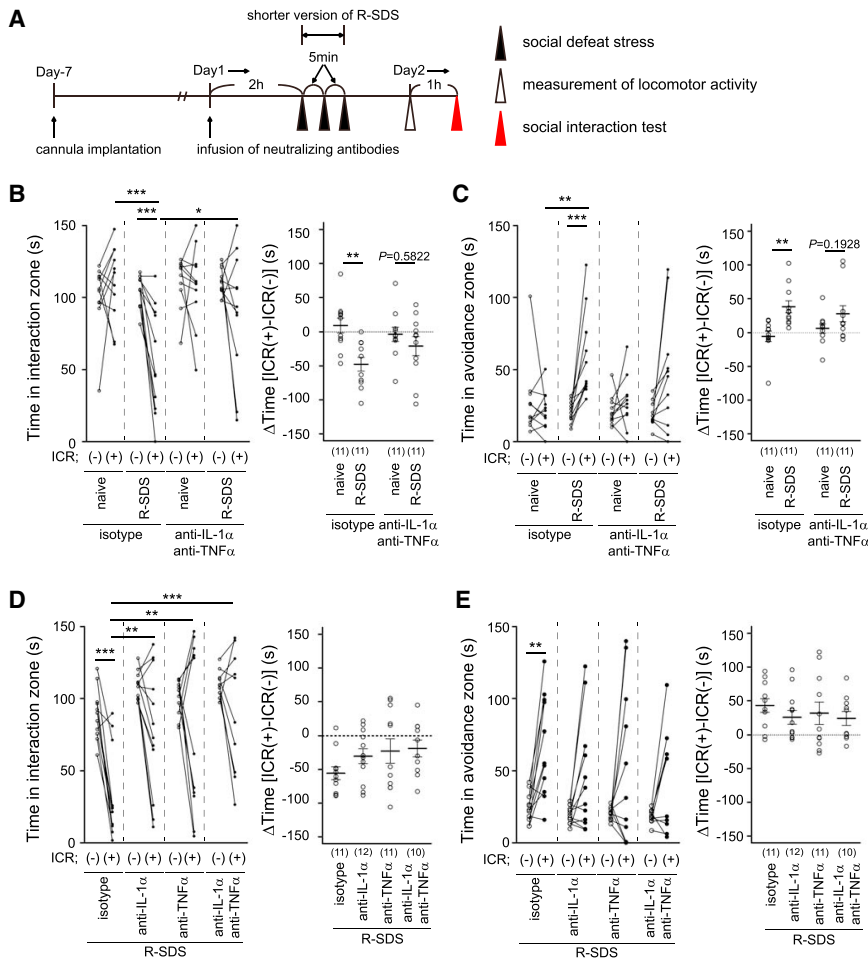
c-Fos expression has frequently been used as a marker for neuronal response to repeated environmental stress (Perrotti et al., 2004; Tanaka et al., 2012). We found that SDS-induced c-Fos expression in mPFC neurons is attenuated after R-SDS

Figure 6. TLR2/4 in mPFC Microglia Are Crucial for R-SDS-Induced Social Avoidance

- (A) Experimental design for mPFC microglia-specific knockdown of TLR2/4.
 - (B) Schedule for behavioral experiments.
 - (C) Representative images of mCherry signals co-expressed with TLR2/4 microRNA in EYFP-positive microglia in the mPFC of CX3CR1-CreER mice infected with the lentiviral vector shown in (A). EYFP and mCherry signals are shown in green and red, respectively. Scale bar, 25 μ m.
 - (D–G) The proportions of mCherry-positive cells in EYFP-expressing cells (D), the proportions of EYFP-positive cells in mCherry-expressing cells (E), the numbers of cells expressing mCherry and EYFP (F), and the numbers of cells expressing mCherry and CD45 (G) in the mPFC of CX3CR1-CreER mice infected with lentiviral vectors expressing control microRNA (Control) and TLR2/4 microRNA (TLR2/4KD) with or without R-SDS (R-SDS or naive, respectively).
 - (H–K) The levels of social interaction (H and J) and social avoidance (I and K) in CX3CR1-CreER mice that received an mPFC injection of the lentiviral vector expressing control microRNA (Control) or TLR2/4 microRNA (TLR2/4KD) with either microRNA-resistant TLR2 or TLR4 mutant (TLR2mt7 or TLR4mt8, respectively) or mCherry with or without prior R-SDS (R-SDS or naive, respectively). The data were analyzed and are shown as in Figures 1C and 1D.
 - (L) The time spent in the open arms in the elevated plus maze test as an index for anxiety in the same mice as in (H) and (I).
 - (M) The numbers of c-Fos-positive mPFC neurons of CX3CR1-CreER mice that received mPFC injections with a lentiviral vector expressing control microRNA (Control, R-SDS(sus)) or TLR2/4 microRNA (TLR2/4KD, R-SDS) 1.5 hr after R-SDS.
- * $p < 0.05$, ** $p < 0.01$, *** $p < 0.001$ for Bonferroni's multiple comparisons test (H, I, and K); * $p < 0.05$ for unpaired t test (M). The number of mice is shown below each group. Data are shown as means \pm SEM. See also Figures S5–S7.



(legend on next page)



in susceptible but not resilient mice. In addition, repeated environmental stress-induced dendritic atrophy in mPFC pyramidal neurons is thought to underlie the concomitant behavioral changes (Dias-Ferreira et al., 2009; Duman and Aghajanian, 2012). Therefore, the TLR2/4-dependent changes in mPFC neurons described above could underlie R-SDS-induced social avoidance.

Figure 7. R-SDS Alters Cytokine Expression in mPFC Microglia in a TLR2/4-Dependent Manner

(A) Design of transcriptome analysis of wild-type or TLR-DKO microglia isolated from the mPFC and NAc without or with R-SDS. Each sample was derived from total RNA from microglia in the mPFC or NAc of 3–6 mice, which was sufficient for transcriptome analysis using the DNA microarray under our experimental conditions.

(B and C) The levels of social interaction (B) and social avoidance (C) in CX3CR1-EGFP mice and TLR-DKO; CX3CR1-EGFP mice with or without R-SDS (R-SDS or naive, respectively). The mice used for this analysis are highlighted in red. The data were analyzed and are shown as in Figures 1C and 1D.

(D and E) Venn diagrams showing the numbers of DNA microarray probes that were significantly upregulated (D) or downregulated (E) by R-SDS in wild-type microglia or TLR-DKO microglia isolated from the mPFC or NAc.

(F and G) A heatmap (F) and bubble charts (G) showing R-SDS-induced changes in gene expression of representative cytokines in microglia isolated from the mPFC and NAc of susceptible wild-type mice (WT_R-SDS(sus)) and TLR-DKO mice (TLR-DKO_R-SDS) compared with those with the respective genotypes without R-SDS (WT_naïve and TLR-DKO_naive, respectively). In the bubble charts, the size of a bubble indicates the expression level of a respective gene in microglia isolated from the mPFC or NAc of susceptible wild-type mice after R-SDS.

(H–K) The expression levels of representative R-SDS-upregulated cytokines—namely, IL-1 α (H), TNF- α (I), IL-1 β (J), and IL-6 (K)—in microglia isolated from the mPFC or NAc of wild-type mice and TLR-DKO mice with or without R-SDS (R-SDS or naive, respectively). Among defeated wild-type mice, only susceptible mice were analyzed (R-SDS(s)).

***p < 0.001 for Bonferroni's multiple comparisons test (B and C); *p < 0.05 for unpaired t test (F and H–J). The number of mice (B and C) or samples (H–K) is shown below each group. Data are shown as means ± SEM. See also Figure S2.

Figure 8. IL-1 α and TNF- α in the mPFC Are Crucial for R-SDS-Induced Social Avoidance

(A) Schedule of behavioral experiments.

(B–E) The levels of social interaction (B and D) and social avoidance (C and E) in wild-type mice that received mPFC infusions with a mixture of neutralizing antibodies (anti-IL-1 α anti-TNF α), either of these antibodies added singly (anti-IL-1 α or anti-TNF α), or control antibodies of the corresponding isotypes (isotype) with or without R-SDS (R-SDS or naive, respectively). The data were analyzed and are shown as in Figures 1C and 1D. *p < 0.05, **p < 0.01, ***p < 0.001 for Bonferroni's multiple comparisons test. The number of mice is shown below each group. Data are shown as means ± SEM. See also Figure S2.

In addition to these changes, our histological analyses of the number of PSD-95 puncta suggest that R-SDS increases the number of excitatory synapses in the deep layer of the mPFC in susceptible wild-type mice in a manner dependent on TLR2/4 expressed in mPFC microglia. This result was unexpected, based on our observations that R-SDS induces dendritic atrophy of mPFC pyramidal neurons (Figures 5F–5H; Shinohara et al., 2017). However, because PSD-95 immunostaining cannot discriminate excitatory synapses on various types of neurons, R-SDS may increase the number of excitatory synapses on some types of neurons other than mPFC pyramidal neurons.

Indeed, it has been reported that chronic restraint stress induces dendritic hypertrophy in a subpopulation of mPFC interneurons identified mainly as Martinotti cells (Gilabert-Juan et al., 2013). It remains to be elucidated whether R-SDS induces distinct types of morphological changes in different types of neurons in the mPFC and whether and how these morphological changes may affect the concomitant behavioral changes.

IL-1 α and TNF- α Are Responsible for the Action of TLR2/4 in mPFC Microglia for R-SDS

We showed that R-SDS significantly induces *Il1a* and *Tnfa* mRNAs in mPFC microglia and marginally in NAc microglia and that administration of their neutralizing antibodies into the mPFC abolishes R-SDS-induced social avoidance. These observations strongly imply that IL-1 α and TNF- α released from activated mPFC microglia are responsible for R-SDS-induced social avoidance. These neutralizing antibodies appeared to inhibit the R-SDS-induced CD68 increase, indicative of microglial activation, in the mPFC. Thus, these cytokines could constitute an autocrine loop for R-SDS-induced microglial activation. It has also been reported that IL-1 α and TNF- α are sufficient to induce neurotoxic reactive astrocytes (Liddelow et al., 2017). TNF receptor type 1 (TNFR1) in astrocytes has been shown to be instrumental in hippocampal synaptic alteration and impaired contextual learning in an animal model of multiple sclerosis (Habbas et al., 2015). Therefore, microglia-derived TNF- α could act on astrocytic TNFR1 to induce R-SDS-induced neuronal and behavioral changes. The mechanism of action of IL-1 α remains elusive. Interestingly, it has been shown that IL-1 α or IL-1 β in combination with TNF- α induces different types of astrocytes (neurotoxic or protective astrocytes, respectively; Liddelow et al., 2017), suggesting different mechanisms of action of IL-1 α and IL-1 β .

We also found that, among three conventional markers for microglial activation, the R-SDS-induced increase in CD68 signals in mPFC microglia was the most correlated with the level of social avoidance. CD68 is a scavenger receptor that is predominantly located at the late endosomal and lysosomal compartments and is thought to be associated with phagocytic activity (Murphy et al., 2005). It has been suggested that microglia engulf synaptic structures into CD68-positive phagosomal compartments for synaptic pruning during postnatal development (Paolicelli et al., 2011; Schafer et al., 2012) and in a mouse model of Alzheimer's disease (Hong et al., 2016). Similarly, R-SDS-activated microglia could also engulf synaptic and dendritic elements of mPFC neurons into CD68-positive phagosomal compartments. It has been shown that astrocyte-derived TGF- β induces C1q expression in retinal ganglion cells, which is crucial for complement- and microglia-dependent synaptic pruning (Bialas and Stevens, 2013). Because it has been reported that IL-1 α and TNF- α induce neurotoxic astrocytes (Liddelow et al., 2017), these cytokines derived from microglia upon R-SDS could alter astrocytic functions to promote synaptic and dendritic engulfment by mPFC microglia.

Conclusions

Collectively, our study demonstrates an unexpected pivotal role of TLR2/4 for R-SDS-induced behavioral changes as well as neuronal and microglial changes in the mPFC and strongly indicates that TLR2/4 in mPFC microglia mediate R-SDS-induced neuronal and behavioral changes through IL-1 α and TNF- α . Therefore, we propose that targeting innate immunity may provide therapeutic benefits for stress-related pathophysiology in psychiatric disorders.

STAR★METHODS

Detailed methods are provided in the online version of this paper and include the following:

- KEY RESOURCES TABLE
- CONTACT FOR REAGENT AND RESOURCE SHARING
- EXPERIMENTAL MODEL AND SUBJECT DETAILS
 - Mice
- METHOD DETAILS
 - Social defeat stress (SDS)
 - Social interaction test
 - Elevated plus maze test
 - Immunostaining
 - Analyses of immunofluorescent images
 - Golgi-Cox staining
 - Isolation of microglia from the brain
 - Quantitative RT-PCR
 - Transplantation of cultured microglia-like cells into the mPFC
 - Lentiviral vectors
 - Knockdown of TLR2/4 in cultured cells
 - Injection of lentiviral vectors into the mPFC
 - Transcriptome analyses
 - Local infusion of neutralizing antibodies into the mPFC
- QUANTIFICATION AND STATISTICAL ANALYSIS
- DATA AND SOFTWARE AVAILABILITY

SUPPLEMENTAL INFORMATION

Supplemental Information includes eight figures and one table and can be found with this article online at <https://doi.org/10.1016/j.neuron.2018.06.035>.

A video abstract is available at <https://doi.org/10.1016/j.neuron.2018.06.035#mmc4>.

ACKNOWLEDGMENTS

We thank Dr. Hiroyuki Hioki for technical advice regarding the generation of lentiviral vectors, Dr. Ryota Shinohara for technical advice regarding the design of microRNA, and Dr. Hirotaka Nagai for technical advice regarding the isolation of microglia by FACS. We also thank Atsushi Mizutani and Nodoka Asamoto for animal care; Tae Arai, Akiko Washimi, and Misako Takizawa for secretarial help; Kimiko Nonomura for technical assistance; and Prof. James Hejna (Kyoto University) for critical reading of the manuscript. This study was supported in part by a CREST grant from JST (JP15gm0410006 to S.N.); a CREST grant from AMED (JP17gm0910012 to T.F.); Grants-in-Aids for Scientific Research 24689015, 16H05132, and 17K19457 (to T.F.) and 17K08593 (to S.K.); Grants-in-Aids for JSPS Research Fellow 15J07561 (to X.N.) and 17J09360 (to M.T.) from the Japan Society for the Promotion of Science; Grants-in-Aids for Scientific Research from the Ministry of Education, Culture, Sports, Science and Technology in Japan (25116517, 25116715, 15H01289, 17H06057, and 17H05572 to T.F.); and research grants from the Uehara Memorial Foundation (to T.F.), the Sumitomo Foundation (to T.F.), the Naito Foundation (to T.F.), the Astellas Foundation for Research on Metabolic Disorders (to T.F.), and the Takeda Science Foundation (to T.F.).

AUTHOR CONTRIBUTIONS

T.F., S.N., and S.K. designed the project. T.F., S.N., S.K., and A.K. wrote the manuscript. X.N. and S.K. performed most experiments. X.N. and K.T. performed behavioral experiments using knockout mice. A.O. and S.K. performed transplantation of microglia-like cells. S.K. generated lentiviral vectors, and X.N., A.T., K.N., and F.N. analyzed knockdown efficiency. F.N. generated

microRNA-resistant TLR2/4 mutant cDNAs and performed behavioral experiments with these mutants. S.K. and X.N. acquired mPFC microglia-specific transcriptome data, and S.K., E.S.-N., and Y.I. analyzed these transcriptome data. X.N. and Y.M.-K. acquired fluorescent images using SIM, and X.N. and M.T. analyzed these images. Project management was carried out by S.K. and T.F.

DECLARATION OF INTERESTS

The authors declare no competing interests.

Received: January 24, 2018

Revised: May 29, 2018

Accepted: June 21, 2018

Published: July 19, 2018

REFERENCES

- Åkerblom, M., Sachdeva, R., Quintino, L., Wettergren, E.E., Chapman, K.Z., Manfre, G., Lindvall, O., Lundberg, C., and Jakobsson, J. (2013). Visualization and genetic modification of resident brain microglia using lentiviral vectors regulated by microRNA-9. *Nat. Commun.* 4, 1770.
- Bagot, R.C., Parise, E.M., Peña, C.J., Zhang, H.X., Maze, I., Chaudhury, D., Persaud, B., Cachope, R., Bolaños-Guzmán, C.A., Cheer, J.F., et al. (2015). Ventral hippocampal afferents to the nucleus accumbens regulate susceptibility to depression. *Nat. Commun.* 6, 7062.
- Bialas, A.R., and Stevens, B. (2013). TGF- β signaling regulates neuronal C1q expression and developmental synaptic refinement. *Nat. Neurosci.* 16, 1773–1782.
- Butovsky, O., Jedrychowski, M.P., Moore, C.S., Cialic, R., Lanser, A.J., Gabriely, G., Koeglsperger, T., Dake, B., Wu, P.M., Doykan, C.E., et al. (2014). Identification of a unique TGF- β -dependent molecular and functional signature in microglia. *Nat. Neurosci.* 17, 131–143.
- Coveney, A.P., Wang, W., Kelly, J., Liu, J.H., Blankson, S., Wu, Q.D., Redmond, H.P., and Wang, J.H. (2015). Myeloid-related protein 8 induces self-tolerance and cross-tolerance to bacterial infection via TLR4- and TLR2-mediated signal pathways. *Sci. Rep.* 5, 13694.
- Dias-Ferreira, E., Sousa, J.C., Melo, I., Morgado, P., Mesquita, A.R., Cerqueira, J.J., Costa, R.M., and Sousa, N. (2009). Chronic stress causes frontostriatal reorganization and affects decision-making. *Science* 325, 621–625.
- Drevets, W.C., Price, J.L., and Furey, M.L. (2008). Brain structural and functional abnormalities in mood disorders: implications for neurocircuitry models of depression. *Brain Struct. Funct.* 213, 93–118.
- Duman, R.S., and Aghajanian, G.K. (2012). Synaptic dysfunction in depression: potential therapeutic targets. *Science* 338, 68–72.
- Frank, M.G., Baratta, M.V., Sprunger, D.B., Watkins, L.R., and Maier, S.F. (2007). Microglia serve as a neuroimmune substrate for stress-induced potentiation of CNS pro-inflammatory cytokine responses. *Brain Behav. Immun.* 21, 47–59.
- Gilabert-Juan, J., Castillo-Gomez, E., Guirado, R., Moltó, M.D., and Nacher, J. (2013). Chronic stress alters inhibitory networks in the medial prefrontal cortex of adult mice. *Brain Struct. Funct.* 218, 1591–1605.
- Giovanolli, S., Engler, H., Engler, A., Richetto, J., Voget, M., Willi, R., Winter, C., Riva, M.A., Mortensen, P.B., Feldon, J., et al. (2013). Stress in puberty unmasks latent neuropathological consequences of prenatal immune activation in mice. *Science* 339, 1095–1099.
- Glaccum, M.B., Stocking, K.L., Charrier, K., Smith, J.L., Willis, C.R., Maliszewski, C., Livingston, D.J., Peschon, J.J., and Morrissey, P.J. (1997). Phenotypic and functional characterization of mice that lack the type I receptor for IL-1. *J. Immunol.* 159, 3364–3371.
- Golden, S.A., Christoffel, D.J., Heshmati, M., Hodes, G.E., Magida, J., Davis, K., Cahill, M.E., Dias, C., Ribeiro, E., Ables, J.L., et al. (2013). Epigenetic regulation of RAC1 induces synaptic remodeling in stress disorders and depression. *Nat. Med.* 19, 337–344.
- Goshen, I., Kreisel, T., Ben-Menachem-Zidon, O., Licht, T., Weidenfeld, J., Ben-Hur, T., and Yirmiya, R. (2008). Brain interleukin-1 mediates chronic stress-induced depression in mice via adrenocortical activation and hippocampal neurogenesis suppression. *Mol. Psychiatry* 13, 717–728.
- Habbas, S., Santello, M., Becker, D., Stubbe, H., Zappia, G., Liaudet, N., Klaus, F.R., Koliatis, G., Fontana, A., Pryce, C.R., et al. (2015). Neuroinflammatory TNF α Impairs Memory via Astrocyte Signaling. *Cell* 163, 1730–1741.
- Hinwood, M., Morandini, J., Day, T.A., and Walker, F.R. (2012). Evidence that microglia mediate the neurobiological effects of chronic psychological stress on the medial prefrontal cortex. *Cereb. Cortex* 22, 1442–1454.
- Hioki, H., Kameda, H., Nakamura, H., Okunomiya, T., Ohira, K., Nakamura, K., Kuroda, M., Furuta, T., and Kaneko, T. (2007). Efficient gene transduction of neurons by lentivirus with enhanced neuron-specific promoters. *Gene Ther.* 14, 872–882.
- Hong, S., Beja-Glasser, V.F., Nfonoyim, B.M., Frouin, A., Li, S., Ramakrishnan, S., Merry, K.M., Shi, Q., Rosenthal, A., Barres, B.A., et al. (2016). Complement and microglia mediate early synapse loss in Alzheimer mouse models. *Science* 352, 712–716.
- Hoshino, K., Takeuchi, O., Kawai, T., Sanjo, H., Ogawa, T., Takeda, Y., Takeda, K., and Akira, S. (1999). Cutting edge: Toll-like receptor 4 (TLR4)-deficient mice are hyporesponsive to lipopolysaccharide: evidence for TLR4 as the Lps gene product. *J. Immunol.* 162, 3749–3752.
- Iwasaki, A., and Medzhitov, R. (2010). Regulation of adaptive immunity by the innate immune system. *Science* 327, 291–295.
- Iwata, M., Ota, K.T., Li, X.Y., Sakaue, F., Li, N., Dutheil, S., Banasr, M., Duric, V., Yamanashi, T., Kaneko, K., et al. (2015). Psychological stress activates the inflammasome via release of adenosine triphosphate and stimulation of the purinergic type 2X7 receptor. *Biol. Psychiatry* 80, 12–22.
- Jung, S., Aliberti, J., Graemmel, P., Sunshine, M.J., Kreutzberg, G.W., Sher, A., and Littman, D.R. (2000). Analysis of fractalkine receptor CX(3)CR1 function by targeted deletion and green fluorescent protein reporter gene insertion. *Mol. Cell. Biol.* 20, 4106–4114.
- Koo, J.W., and Duman, R.S. (2008). IL-1beta is an essential mediator of the antineurogenic and anhedonic effects of stress. *Proc. Natl. Acad. Sci. USA* 105, 751–756.
- Kreisel, T., Frank, M.G., Licht, T., Reshef, R., Ben-Menachem-Zidon, O., Baratta, M.V., Maier, S.F., and Yirmiya, R. (2014). Dynamic microglial alterations underlie stress-induced depressive-like behavior and suppressed neurogenesis. *Mol. Psychiatry* 19, 699–709.
- Krishnan, V., Han, M.H., Graham, D.L., Berton, O., Renthal, W., Russo, S.J., Laplant, Q., Graham, A., Lutter, M., Lagace, D.C., et al. (2007). Molecular adaptations underlying susceptibility and resistance to social defeat in brain reward regions. *Cell* 131, 391–404.
- Krishnan, V., and Nestler, E.J. (2008). The molecular neurobiology of depression. *Nature* 455, 894–902.
- Li, N., Liu, R.J., Dwyer, J.M., Banasr, M., Lee, B., Son, H., Li, X.Y., Aghajanian, G., and Duman, R.S. (2011). Glutamate N-methyl-D-aspartate receptor antagonists rapidly reverse behavioral and synaptic deficits caused by chronic stress exposure. *Biol. Psychiatry* 69, 754–761.
- Liddelow, S.A., Guttenplan, K.A., Clarke, L.E., Bennett, F.C., Bohlen, C.J., Schirmer, L., Bennett, M.L., Münch, A.E., Chung, W.S., Peterson, T.C., et al. (2017). Neurotoxic reactive astrocytes are induced by activated microglia. *Nature* 541, 481–487.
- McEwen, B.S., and Morrison, J.H. (2013). The brain on stress: vulnerability and plasticity of the prefrontal cortex over the life course. *Neuron* 79, 16–29.
- McKim, D.B., Patterson, J.M., Wohleb, E.S., Jarrett, B.L., Reader, B.F., Godbout, J.P., and Sheridan, J.F. (2016). Sympathetic Release of Splenic Monocytes Promotes Recurring Anxiety Following Repeated Social Defeat. *Biol. Psychiatry* 79, 803–813.
- Murphy, J.E., Tedbury, P.R., Homer-Vanniasinkam, S., Walker, J.H., and Ponnambalam, S. (2005). Biochemistry and cell biology of mammalian scavenger receptors. *Atherosclerosis* 182, 1–15.

- Ota, K.T., Liu, R.J., Voleti, B., Maldonado-Aviles, J.G., Duric, V., Iwata, M., Dutheil, S., Duman, C., Boikess, S., Lewis, D.A., et al. (2014). REDD1 is essential for stress-induced synaptic loss and depressive behavior. *Nat. Med.* 20, 531–535.
- Paolicelli, R.C., Bolasco, G., Pagani, F., Maggi, L., Scianni, M., Panzanelli, P., Giustetto, M., Ferreira, T.A., Guiducci, E., Dumas, L., et al. (2011). Synaptic pruning by microglia is necessary for normal brain development. *Science* 333, 1456–1458.
- Parkhurst, C.N., Yang, G., Ninan, I., Savas, J.N., Yates, J.R., 3rd, Lafaille, J.J., Hempstead, B.L., Littman, D.R., and Gan, W.B. (2013). Microglia promote learning-dependent synapse formation through brain-derived neurotrophic factor. *Cell* 155, 1596–1609.
- Paxinos, G., and Franklin, K.B. (2003). *The Mouse Brain in Stereotaxic Coordinates*, Second Edition (Academic Press).
- Perrotti, L.I., Hadeishi, Y., Ulery, P.G., Barrot, M., Monteggia, L., Duman, R.S., and Nestler, E.J. (2004). Induction of deltaFosB in reward-related brain structures after chronic stress. *J. Neurosci.* 24, 10594–10602.
- Rivest, S. (2009). Regulation of innate immune responses in the brain. *Nat. Rev. Immunol.* 9, 429–439.
- Schafer, D.P., Lehrman, E.K., Kautzman, A.G., Koyama, R., Mardinaly, A.R., Yamasaki, R., Ransohoff, R.M., Greenberg, M.E., Barres, B.A., and Stevens, B. (2012). Microglia sculpt postnatal neural circuits in an activity and complement-dependent manner. *Neuron* 74, 691–705.
- Shinohara, R., Taniguchi, M., Ehrlich, A.T., Yokogawa, K., Deguchi, Y., Cherasse, Y., Lazarus, M., Urade, Y., Ogawa, A., Kitaoka, S., et al. (2017). Dopamine D1 receptor subtype mediates acute stress-induced dendritic growth in excitatory neurons of the medial prefrontal cortex and contributes to suppression of stress susceptibility in mice. *Mol. Psychiatry*. <https://doi.org/10.1038/mp.2017.177>.
- Takeuchi, O., Hoshino, K., Kawai, T., Sanjo, H., Takada, H., Ogawa, T., Takeda, K., and Akira, S. (1999). Differential roles of TLR2 and TLR4 in recognition of gram-negative and gram-positive bacterial cell wall components. *Immunity* 11, 443–451.
- Tanaka, K., Furuyashiki, T., Kitaoka, S., Senzai, Y., Imoto, Y., Segi-Nishida, E., Deguchi, Y., Breyer, R.M., Breyer, M.D., and Narumiya, S. (2012). Prostaglandin E2-mediated attenuation of mesocortical dopaminergic pathway is critical for susceptibility to repeated social defeat stress in mice. *J. Neurosci.* 32, 4319–4329.
- Tornatzky, W., and Miczek, K.A. (1993). Long-term impairment of autonomic circadian rhythms after brief intermittent social stress. *Physiol. Behav.* 53, 983–993.
- Tsuda, M., Shigemoto-Mogami, Y., Koizumi, S., Mizokoshi, A., Kohsaka, S., Salter, M.W., and Inoue, K. (2003). P2X4 receptors induced in spinal microglia gate tactile allodynia after nerve injury. *Nature* 424, 778–783.
- Vogl, T., Tenbrock, K., Ludwig, S., Leukert, N., Ehrhardt, C., van Zoelen, M.A., Nacken, W., Foell, D., van der Poll, T., Sorg, C., and Roth, J. (2007). Mrp8 and Mrp14 are endogenous activators of Toll-like receptor 4, promoting lethal, endotoxin-induced shock. *Nat. Med.* 13, 1042–1049.
- Wohleb, E.S., Hanke, M.L., Corona, A.W., Powell, N.D., Stiner, L.M., Bailey, M.T., Nelson, R.J., Godbout, J.P., and Sheridan, J.F. (2011). β -Adrenergic receptor antagonism prevents anxiety-like behavior and microglial reactivity induced by repeated social defeat. *J. Neurosci.* 31, 6277–6288.
- Wohleb, E.S., Powell, N.D., Godbout, J.P., and Sheridan, J.F. (2013). Stress-induced recruitment of bone marrow-derived monocytes to the brain promotes anxiety-like behavior. *J. Neurosci.* 33, 13820–13833.

STAR★METHODS

KEY RESOURCES TABLE

REAGENT or RESOURCE	SOURCE	IDENTIFIER
Antibodies		
Rabbit polyclonal anti-c-Fos	Merck; Millipore	Cat#PC38-100μl; RRID: AB_2314043
Rabbit polyclonal anti- Iba-1	Wako	Cat#019-19741; RRID: AB_839504
Mouse monoclonal anti-NeuN	Chemicon	Cat#MAB377; RRID: AB_2298772
Rat monoclonal anti-CD68	AbD serotec	Cat#ABD-MCA1957; RRID: AB_322219
Mouse monoclonal anti-CD68	Abcam	Cat#ab955; RRID: AB_307338
Rat monoclonal anti-CD45	AbD serotec	Cat# ABD-MCA1388; RRID: AB_321729
Rat monoclonal anti-CD11b	AbD serotec	Cat#ABD-MCA711FT-25; RRID: AB_323135
Rat monoclonal anti-GFP	Nacalai	Cat#04404-84; RRID: AB_10013361
Rabbit polyclonal anti-RFP	Rockland,	Cat#600-401-379; RRID: AB_2209751
Mouse monoclonal anti-RFP	MBL	Cat#M165-3; RRID: AB_1520843
Rat monoclonal anti-HA	Roche	Cat#11867423001; RRID: AB_10094468
Mouse monoclonal anti-FLAG	Sigma-Aldrich	Cat#F1804; RRID: AB_262044
Rabbit monoclonal anti-synaptophysin	Abcam	Cat# AB16659-1; RRID: AB_443419
Mouse monoclonal anti-PSD-95	Merck; Millipore	Cat#MAB1596; RRID: AB_2092365
Armenian hamster monoclonal anti-IL-1 alpha	eBioscience,	Cat#16-7011-85; RRID: AB_469199
Rat monoclonal anti-TNF-α	BioLegend,	Cat#506331; RRID: AB_11147367
Bacterial and Virus Strains		
pLV-PGK-GFP	Dr. Johan Jakobsson	N/A
Lenti-X HTX packaging System	Clontech	Cat#631247
Chemicals, Peptides, and Recombinant Proteins		
blastcidin	Wako	Cat#029-18701; CAS: 3513-03-9
Armenian Hamster IgG Isotype Control	eBioscience	Cat#16-4888-85; RRID: AB_470172
Rat IgG1, κ Isotype Ctrl Antibody	BioLegend	Cat#400431; RRID: AB_11150233
Critical Commercial Assays		
FD Rapid GolgiStain Kit	FD Neuro Technologies	Cat# PK401
Ovation RNA Amplification System V2	NuGEN	Cat#3100-12
Low Input Quick Amp Labeling Kit	Agilent Technologies	Cat#5190-2305
SurePrint G3 Mouse GE 8×60K Microarray	Agilent Technologies	Cat#G4852B
Deposited Data		
Raw microarray data	This paper	GSE115996
Experimental Models: Cell Lines		
Mouse: N9 cells	Laboratory of Dr. Makoto Tsuda	RRID: CVCL_0452
Human: Lenti-X 293T cells	Clontech	Cat#632180; RRID: CVCL_4401
Experimental Models: Organisms/Strains		
Mouse: TLR2 knockout mice	Oriental Bio Service	RRID: IMSR_OBS:3
Mouse: TLR4 knockout mice	Oriental Bio Service	RRID: IMSR_OBS:4
Mouse: B6.129S7-Il1rltm1Imx/J	The Jackson Laboratory	RRID: IMSR_JAX:003245
Mouse: B6.129P-Cx3cr1tm1Litt/J	The Jackson Laboratory	RRID: IMSR_JAX:005582
Mouse: B6.129P2(Cg)-Cx3cr1tm2.1(cre/ERT2)Litt/WganJ	The Jackson Laboratory	RRID: IMSR_JAX:021160

(Continued on next page)

Continued

REAGENT or RESOURCE	SOURCE	IDENTIFIER
Oligonucleotides		
Primers for quantitative RT-PCR, see Supplemental Experimental Procedures	This paper	N/A
miRNA target sequence, see Supplemental Experimental Procedures	This paper	N/A
Recombinant DNA		
mTLR1	Addgene	Cat #13080
pCMV-SPORT-mTLR2	Dharmacon	Cat#MMM1013-202763576
pCMV-SPORT6-mTLR3	Dharmacon	Cat#MMM1013-202709109
pCMV-SPORT6-mTLR4	Dharmacon	Cat#MMM1013-202761834
pCR-BluntII-TOPO-mTLR5	Dharmacon	Cat#MMM1013-211692986
pCMV-SPORT6-mTLR6	Dharmacon	Cat#MMM1013-202709109
pCR4-TOPO-mTLR7	Dharmacon	Cat#MMM1013-211691472
mTLR8 cDNA Plasmid	R&D SYSTEMS	Cat# RDC0786
mTLR9	Addgene	Cat#13091
pCR-BluntII-TOPO-mTLR11	Dharmacon	Cat#MMM1013-211692974
pCR4-TOPO-mTLR12	Dharmacon	Cat#MMM1013-211691876
pCR-BluntII-TOPO-mTLR13	Dharmacon	Cat#MMM1013-211693738
Software and Algorithms		
BZ-II Measurement Module software	Keyence	RRID: SCR_016348
Imaris	Bitplane	RRIDSCR_007370
MetaMorph	Molecular Devices	RRIDSCR_002368
BLOCK-iT RNAi Designer	Thermo Fisher Scientific	https://rnaidesigner.thermofisher.com/rnaiexpress/
PRISM 7.0 software	GraphPad	RRIDSCR_002798

CONTACT FOR REAGENT AND RESOURCE SHARING

Further information and requests for reagents may be directed to, and will be fulfilled by, the Lead Contact and corresponding author, Tomoyuki Furuyashiki (tfuruya@med.kobe-u.ac.jp).

EXPERIMENTAL MODEL AND SUBJECT DETAILS**Mice**

Tlr2 knockout (TLR2-KO) mice (RRID: IMSR_OBS:3) (Takeuchi et al., 1999), *Tlr4* knockout (TLR4-KO) mice (RRID:IMSR_OBS:4) (Hoshino et al., 1999) and *Tlr2/4* double knockout (TLR-DKO) mice in a C57BL/6N background were purchased from Oriental Bio Service. To make all the mice congenic to the C57BL/6N strain, these mice were backcrossed with C57BL/6N mice more than 10 times. These congenic TLR2-KO and TLR4-KO mice were used to generate TLR-DKO mice. From the crossing among TLR2-KO, TLR4-heterozygous mice (*Tlr2(−/−);Tlr4(+/-)*), only TLR2-KO (*Tlr2(−/−);Tlr4(+/+)*) and TLR-DKO (*Tlr2(−/−);Tlr4(−/−)*) littermates (but not TLR2-KO, TLR4-heterozygous (*Tlr2(−/−);Tlr4(+/-)*) littermates) were used. Likewise, only TLR4-KO (*Tlr2(+/+);Tlr4(−/−)*) and TLR-DKO (*Tlr2(−/−);Tlr4(−/−)*) littermates (but not TLR2-heterozygous, TLR4-KO (*Tlr2(+/-);Tlr4(−/−)*) littermates) were used from the crossing among TLR2-heterozygous, TLR4-KO mice. *Il1r1* knockout (IL-1RI-KO) mice (formally named B6.129S7-Il1r1tm1lmx/J (RRID:IMSR_JAX:003245)) (Glaccum et al., 1997), CX3CR1-EGFP mice (formally named B6.129P-Cx3cr1tm1Litt/J (RRID:IMSR_JAX:005582)) (Jung et al., 2000) and Cx3cr1-CreER mice (formally named B6.129P2(Cg)-Cx3cr1tm2.1(cre/ERT2)Litt/WganJ (RRID:IMSR_JAX:021160)) (Parkhurst et al., 2013) in the C57BL/6 strain background were purchased from Jackson Laboratory. Adult male C57BL/6N mice and male ICR mice retired from breeding were purchased from Japan SLC and CLEA Japan, respectively. Mice were housed in a group of four mice in a specific pathogen-free and temperature- and humidity-controlled vivarium under a 12-h light, 12-h dark cycle (light on between 0800 and 2000) with free access to chow and water. All procedures for animal care and use were in accordance with the National Institutes of Health Guide for the Care and Use of Laboratory Animals and were approved by the Animal Care and Use Committees of Kyoto University Graduate School of Medicine and Graduate School of Pharmaceutical Sciences and Kobe University Graduate School of Medicine.

METHOD DETAILS

Social defeat stress (SDS)

Single SDS (S-SDS) or repeated SDS (R-SDS) was applied as described previously (Tanaka et al., 2012) with minor modifications. Briefly, male ICR mice were screened based on their aggressiveness to a male C57BL/6N mouse, as measured by the latency and the number of attacks during the observation period (180 s), and were used as aggressor mice for SDS. Before SDS, 6~12-week-old male mice, were isolated with free access to chow and water for 1 week. Each of the isolated mice to be defeated was introduced and kept in the home cage of a resident aggressor ICR mouse for 10 min daily for 1 day (S-SDS) or 10 consecutive days (R-SDS), except that R-SDS was applied for 4 consecutive days (R-SDS for 4 days) in Figures 3K, 3L, S3F, S3G, and S5D–S5G. The pairs of defeated and aggressor mice were randomized daily to minimize the variability in the aggressiveness of aggressor mice. To examine the time spent for a submissive posture during SDS, behaviors of mice were video-recorded during SDS and analyzed post hoc in a manner blind to the mouse genotype. A submissive posture was defined as a posture of a defeated mouse standing upright with the belly exposed to an aggressor (Tornatzky and Miczek, 1993). SDS was applied between 1600 and 1900 h in a sound-attenuated room in dim light. Control mice were placed in a novel cage for 10 min daily for the same number of days as R-SDS. Each mouse was subjected to the social interaction test and the elevated plus maze test consecutively, with or without prior R-SDS. In Figure 8, to reduce the amounts of antibodies to be used, we employed a shorter version of R-SDS, which is composed of three exposures to social defeat for 10 min each, with 5 min intervals between each exposure.

Social interaction test

The social interaction test was performed as previously described (Tanaka et al., 2012), with minor modifications. A defeated or control mouse was kept for 150 s in an open field chamber (30 cm × 40 cm) with a wire mesh cage (10 cm × 6 cm) enclosing an unfamiliar ICR mouse located at one end of the field. Mouse behaviors were video-monitored, and the trajectory of mouse ambulation was automatically determined and recorded by a SMART video tracking system (Harvard Apparatus). A 30 cm × 15 cm rectangular zone including the wire mesh cage was defined as the social interaction zone (Figure 1B). A 30 cm × 9 cm rectangular zone opposite to the social interaction zone was defined as the social avoidance zone. The durations which each mouse spent in the respective zones were used as indices for the levels of social interaction and social avoidance, respectively. One day before the social interaction test, mice were habituated to the test chamber without an ICR mouse, except in Figure 8, in which the habituation and the social interaction test were performed on the same day. Traveling distances during this habituation period were used to define novelty-induced locomotor activity. The social interaction test was performed between 1500 and 1700 h on the following days after R-SDS for 4 or 10 days, unless otherwise stated.

It has been reported that the level of social avoidance varies considerably across individual mice. In this study, we defined susceptible mice as those which showed social interaction and social avoidance for less than 40% and more than 60%, respectively, of the observation period. Resilient mice were defined as those which showed social interaction and social avoidance for more than 60% and less than 40%, respectively, of the observation period. These criteria excluded mice that spent most of the time in the middle zone and were thus difficult to categorize as either susceptible or resilient. Indeed, susceptible and resilient wild-type mice comprised most (77.8%) of the total of defeated wild-type mice prepared for the immunostaining (18/45 and 17/45, respectively).

Elevated plus maze test

The elevated plus maze test was performed as previously described (Tanaka et al., 2012), with minor modifications. An elevated plus maze is composed of two open arms (5 cm wide, 25 cm long, without walls) and two closed arms (5 cm wide, 25 cm long, with 15 cm walls) that are interconnected by a central area of 5 cm square, and it is maintained at a height of 50 cm from the floor. After acclimation to a test environment, a defeated or control mouse was transferred to the center of the elevated plus maze and kept on the maze for 5 min. Mouse behaviors were video-monitored, and the trajectory of mouse ambulation was automatically determined and recorded by the SMART video tracking system (Harvard Apparatus). The proportion of the time that the mouse spent in the open arms during the observation period was determined.

Immunostaining

Immunofluorescent staining for c-Fos, Iba-1, CD68, CD11b, CD45, synaptophysin, and PSD-95 in the brain was performed without SDS, or at 1.5 h and 4 h after S-SDS or the last session of R-SDS. Susceptible mice and resilient mice were chosen according to the social interaction test after the last session of R-SDS for 10 days, and were subjected to an additional SDS at 1.5 h and 4 h prior to sacrifice. Immunofluorescent staining was performed as described previously (Tanaka et al., 2012) with minor modifications. Briefly, under deep anesthesia with intraperitoneal (i.p.) injection of sodium pentobarbital (50 mg/kg; Nacalai), mice were transcardially perfused with 20 mL Dulbecco's modified phosphate buffered saline (D-PBS) followed by 0.1M sodium phosphate buffer (pH 7.4) containing 4% paraformaldehyde. Brains were immersed in 0.1M sodium phosphate buffer (pH 7.4) containing 4% paraformaldehyde and 30% sucrose for 24 h. After the brains were rapidly frozen in OCT compound (Sakura Finetek), coronal brain sections of 30- μ m thickness were made with a cryostat (Carl Zeiss Microlmaging). Immunofluorescent staining for HA tag and FLAG tag in cultured cells was performed as described below. The cells were washed with D-PBS and fixed with 0.1M sodium phosphate buffer

(pH 7.4) containing 4% paraformaldehyde at RT for 30 min. After washed with D-PBS, the brain sections or the cells were incubated in blocking buffer composed of D-PBS containing 0.3% Triton X-100, 1% normal donkey serum and 0.125% carrageenan for 60 min at room temperature (RT). The sections or the cells were then incubated with appropriate primary antibodies in the blocking buffer at 4°C for 36 h. The primary antibodies used in this study were rabbit polyclonal anti-c-Fos (1:5000 dilution, Ab-5; Millipore, RRID: AB_2314043), rabbit anti-Iba-1 (1:500 dilution, 019-19741; Wako, RRID: AB_839504), mouse anti-NeuN (1:500 dilution, MAB377; Chemicon, RRID: AB_2298772), rat anti-CD68 (1:200 dilution, FA-11; AbD serotec, RRID: AB_322219), mouse anti-CD68 (1:500 dilution, KP1; Abcam, RRID: AB_307338), rat anti-CD45 (1:500 dilution, IBL-3/1; AbD serotec, RRID: AB_321729), rat anti-CD11b (1:500 dilution, 5C6; AbD serotec, RRID: AB_323135), rat anti-GFP (1:500 dilution, 04404-84, Nacalai, RRID: AB_10013361), rabbit anti-RFP (1:500 dilution, 600-401-379; Rockland, RRID: AB_2209751), mouse anti-RFP (1:500 dilution, M165-3; MBL, RRID: AB_1520843), rat anti-HA (1:500 dilution, 11867423001; Roche, RRID: AB_10094468), mouse anti-FLAG (1:1000 dilution, F1804; Sigma-Aldrich, RRID: AB_262044), rabbit anti-synaptophysin (1:1000 dilution, AB16659-1; Abcam, RRID: AB_443419) and mouse anti-PSD-95 (1:1000 dilution, MAB1596; Merck Millipore, RRID: AB_2092365). The sections were washed for 10 min three times at RT in D-PBS containing 0.3% Triton X-100. For immunofluorescent staining, the sections or the cells were incubated with Alexa Fluor 488-, Alexa Fluor 555- or Alexa Fluor 647-labeled secondary antibodies (1:500 dilution; Life Technologies) for 2 h at RT. The sections were mounted on APS-coated glass slides (Matsunami Glass). The sections or the cells were embedded in ProLong Gold Antifade Reagent (Life Technologies).

Analyses of immunofluorescent images

Immunofluorescent images for c-Fos staining were acquired through a 10x objective lens (N.A. 0.45) with a BIOREVO HS All-in-one Fluorescence Microscope (Keyence). Immunofluorescent images for synaptophysin and PSD-95 staining were acquired through a 63x oil-immersion objective lens (N.A. 1.40) and processed with channel alignment using structured illumination microscopy (ELYRA PS.1, Carl Zeiss). Fluorescent images for the other signals were acquired through a 40x oil-immersion objective lens (N.A. 1.25) with a TCS-SP5 laser-scanning confocal microscope (Leica Microsystems). Confocal images were obtained at multiple Z planes and vertically projected. Six representative images for mPFC and 4 images for NAc were taken from each mouse. Images for c-Fos signals were analyzed using BZ-II Measurement Module software (Keyence). Images for synaptophysin and PSD-95 were processed using Imaris (Bitplane). Images for the other signals were analyzed using MetaMorph (Molecular Devices). Predetermined thresholds for the intensity and the size were applied to images to detect Iba-1-positive cells, CD68-positive puncta, CD11b-positive puncta, CD45-positive cells, c-Fos-positive nuclei, EYFP-positive cells, mCherry-positive cells, synaptophysin-positive puncta, and PSD-95-positive puncta as objects for subsequent image analyses. The same thresholds were applied to all the images in the same comparison groups. Most c-Fos signals detected using this method merged with DAPI-stained and NeuN-positive nuclei, indicating nuclear c-Fos staining of mPFC neurons (see Figure 5A). The intensity of immunofluorescent Iba-1 signals, the area of CD68-positive puncta, the intensity of CD11b-positive puncta, the number of c-Fos positive nuclei, the number of synaptophysin-positive puncta, and the number of PSD-95-positive puncta were determined for each image. The values of Iba-1 and CD11b intensities were normalized to those of corresponding control groups in respective figures. The numbers of EYFP-positive cells, mCherry-positive cells, CD45-positive cells, EYFP:mCherry-double-positive cells and CD45:mCherry-double-positive cells, as well as the proportion of EYFP:mCherry-double-positive cells in either mCherry-positive cells or EYFP-positive microglia were determined for each image. The resultant values were averaged for respective brain areas of each mouse and statistically analyzed. For χ^2 analysis on the proportions of defeated wild-type and TLR-DKO mice with CD68 and c-Fos signals beyond the distributions of these signals in naive mice, the threshold was determined to maximally discriminate the distributions of each signal between naive and defeated mice of the respective genotypes.

Golgi-Cox staining

Golgi-Cox staining was performed using a FD Rapid GolgiStain Kit (FD Neuro Technologies) according to the manufacturer's instructions. Briefly, mice were sacrificed by decapitation at 24 h after the social interaction test, and the brains were quickly collected in MilliQ water. The anterior part of the brain was dissected and immersed in freshly prepared Golgi-Cox impregnation buffer included in the kit. The impregnation buffer was refreshed after 24 h, and the brains were incubated for 2 weeks. After cryoprotection with the cryoprotectant buffer included in the kit at 4°C for 1 week, each brain was frozen in isopentane kept at -80°C and cut into 200- μ m sections with a cryostat (Carl Zeiss Microlimaging). The sections were mounted on gelatin-coated slides, dried at RT for 72 h, and stained according to the manufacturer's instructions. The sections were counterstained with Nissl staining. The slides were dehydrated in ethanol, cleared in xylene, and covered with Mount Quick (Daido Sangyo). Images were acquired with a BIOREVO HS All-in-one Fluorescence Microscope (Keyence). The lengths of apical dendrites of Golgi-impregnated pyramidal neurons in the mPFC were measured by ImageJ software post hoc in a manner blind to experimental conditions. Since many layer 6 pyramidal neurons possess short apical dendrites, which are much easier to trace than those of other neuronal populations, we chose layer 6 pyramidal neurons for this analysis.

Isolation of microglia from the brain

Since CX3CR1-EGFP mice were generated by replacing the open reading frame for CX3CR1 by that for EGFP (Jung et al., 2000), we used heterozygous CX3CR1-EGFP mice to preserve CX3CR1 function. Cell dissociation from the brain tissue was performed using

the Papain Dissociation System (Worthington Biochemical Corporation). Briefly, under deep anesthesia with i.p. injection of sodium pentobarbital (50 mg/kg; Nacalai), CX3CR1-EGFP mice were transcardially perfused with D-PBS, and the brains were rapidly isolated. After the olfactory bulb and the cerebellum were removed, the brains were minced in Earle's Buffer containing papain and DNase I saturated with 95% O₂ and 5% CO₂ according to the manufacturer's protocol. The small brain tissues were incubated for 60 min at 37°C with rocking and triturated. The dissociated cells were passed through a cell strainer with 70-μm pores (BD Falcon). Myelin was removed using AutoMACS (Miltenyi Biotech) and myelin removal beads (Miltenyi Biotech). Cells were stained with propidium iodide (eBioscience) and subjected to cell sorting using a FACS AriaIII (BD Biosciences). EGFP-positive cells containing microglia and monocytes (a minor population) in the brain, and EGFP-negative cells containing other types of cells were collected. Dead cells were removed according to propidium iodide staining. Total RNA was extracted from the collected cells using an RNeasy Plus Mini kit (QIAGEN).

Quantitative RT-PCR

cDNA was obtained from total RNA using a High Capacity cDNA Reverse Transcription Kit (Life Technologies). All PCR experiments were conducted in duplicate using SYBR Premix Ex Taq (Takara Bio), and fluorescent SYBR Green signals were automatically detected and analyzed with a CFX96 Touch Real-Time PCR Detection System (Bio-Rad) or Applied Biosystems 7500 (Applied Biosystems). Primers for PCR are as follows: for mouse *Actb* (β-actin), 5'-TGC GTG ACA TCA AAG AGA AG-3' and 5'-GAT GCC ACA GGA TTC CAT A-3'; for mouse *Cd11b*, 5'-CAA TAG CCA GCC TCA GTG C-3' and 5'-GAG CCC AGG GGA GAA GTG-3'; for mouse *Tlr1*, 5'-CTG AGG GTC CTG ATA ATG TCC T-3' and 5'-GAT GCC ACA GGA TTC CAT A-3'; for mouse *Tlr2*, 5'-TGG AAT GTC ACC AGG CTG C-3' and 5'-GTC CGT GGA AAT GGT GGC-3'; for mouse *Tlr3*, 5'-GAT ACA GGG ATT GCA CCC ATA-3' and 5'-TCC CCC AAA GGA GTA CAT TAG A-3'; for mouse *Tlr4*, 5'-ATG GAA AAG CCT CGA ATC CT-3' and 5'-TCC AAG TTG CCG TTT CTT GT-3'; for mouse *Tlr5*, 5'-GGC TGT AAC CTC ACC CAG AT-3' and 5'-CCA GGA GTG GAA ATG ATG TG-3'; for mouse *Tlr6*, 5'-ACC GTC AGT GCT GGA AAT AGA-3' and 5'-CGA TGG GTT TTC TGT CTT GG-3'; for mouse *Tlr7*, 5'-CTC CAG TCT TTC TGT ATT GCA CA-3' and 5'-GAA GTT AGT GCC AAG GTC AAG AA-3'; for mouse *Tlr8*, 5'-AAA TCC CAA ATG GAG CAT TC-3' and 5'-CAG CAA GTG AAG GTG AGG AA-3'; for mouse *Tlr9*, 5'-GAG AAT CCT CCA TCT CCC AAC-3' and 5'-CCA GAG TCT CAG CCA GCA C-3'; for mouse *Tlr11*, 5'-ATG GGG CTT TAT CCC TTT TG-3' and 5'-AGA TGT TAT TGC CAC TCA ACC A-3'; for mouse *Tlr12*, 5'-TCT GAG GGG TAA GGG AGA CA-3' and 5'-GCA GTG GGA CAC GAA TAC ATC-3'; for mouse *Tlr13*, 5'-ACT TGG CCG GAC AGT GTT-3' and 5'-GCC CAA CGC ATT TCT GAT-3'; for human *Actb* (β-actin), 5'-ATT GGC AAT GAG CGG TTC-3' and 5'-CGT GGA TGC CAC AGG ACT-3'. The values were normalized to those of β-actin mRNA in the same cDNA samples. The levels were then normalized to those of the control groups.

Transplantation of cultured microglia-like cells into the mPFC

Primary microglia were isolated as microglia-like cells, as described previously (Tsuda et al., 2003). Briefly, brains were removed from the skulls of wild-type neonates at postnatal day 2, and cortices were collected. The cortices were mashed by a cell scraper and passed through a cell strainer with 70-μm pores (BD Falcon). The cells were seeded in a 75-cm² flask and incubated at 37°C and 5% CO₂. After 7–10 days, floating microglia were collected from cultures by shaking a flask at 125 rpm for 60 min and plated on a new culture dish. After the incubation at 37°C and 5% CO₂ for 30 min, culture medium was changed to remove unattached non-microglial cells, and adherent cells were maintained until transplantation. Immunofluorescent staining confirmed that more than 90% of adherent cells were Iba-1-positive cells. On the day of transplantation, adherent cells were collected by a cell scraper. The cell suspension was adjusted to 10,000 cells/μl with Hank's Balanced Salt Solution (HBSS; Life Technologies). The cell suspension of 500 nL per injection site was injected bilaterally into the mPFC through a 27-gauge stainless needle attached to a syringe pump (Eicom) while mice were kept under anesthesia with isoflurane (Wako). The stereotaxic coordinates were targeted to the infralimbic cortex: 1.9 mm anterior from the bregma, 0.4 mm lateral from the midline, and 3.0 mm ventral from the skull surface at the bregma according to a mouse brain atlas (Paxinos and Franklin, 2003). To visualize the distribution of injected microglia, microglia were labeled with carboxyfluorescein diacetate succinimidyl ester (CFSE; Life Technologies) before transplantation. Sham-operated mice received the same treatment, except that HBSS was injected into the mPFC. After a four-week recovery, the mice were subjected to R-SDS for 4 or 10 days. The transplanted cells typically spread around 500 μm from the injection site. The percentage of CFSE/Iba-1 cells over total Iba1 cells was about 50% around the injection site, regardless of whether wild-type or TLR-DKO microglia were transplanted, or whether the mice were defeated or not.

Lentiviral vectors

A lentiviral vector expressing artificial microRNA targeting TLR2/4 with mCherry only in cells expressing Cre recombinase was generated as follows. We designed the sequences for the artificial microRNAs for *Tlr2* and *Tlr4* according to the website for the BLOCK-iT RNAi Designer (Thermo Fisher Scientific). First, the DNA fragment encoding microRNA (miR) for either *Tlr2* (5'-TGC TGT GAA GAG TCA GGT GAT GGA TGG TTT TGG CCA CTG ACT GAC CAT CCA TCC TGA CTC TTC A-3' and 5'-CCT GTG AAG AGT CAG GAT GGA TGG TCA GTC AGT GGC CAA AAC CAT CCA TCA CCT GAC TCT TCA C-3') or *Tlr4* (5'-TGC TGT TCA CGT AGA AAC TGT AAG TCG TTT TGG CCA CTG ACT GAC GAC TTA CAT TCT ACG TGA A-3' and 5'-CCT GTT CAC GTA GAA TGT AAG TCG TCA GTC AGT GGC CAA AAC GAC TTA CAG TTT CTA CGT GAA C-3') was subcloned into pcDNA6.2-GW/EmGFP-miR (Life Technologies). The resultant vectors were named pcDNA6.2-GW/EmGFP-TLR2miR and pcDNA6.2-GW/EmGFP-TLR4miR, respectively. The open reading frame

of EmGFP in pcDNA6.2-GW/EmGFP-TLR4miR was replaced with that of mCherry to generate pcDNA6.2-GW/mCherry-TLR4miR. The fragment encoding *Tlr2*miR was obtained from pcDNA6.2-GW/EmGFP-TLR2miR and inserted between the BgIII and Xhol sites downstream of *Tlr4*miR of pcDNA6.2-GW/mCherry-TLR4miR. The fragment encoding mCherry plus *Tlr4*miR and *Tlr2*miR in tandem (TLR2/4 microRNA) was obtained from the resultant construct and inserted between Ascl and Nhel sites of pAAV-EF1 α -DIO-EYFP vector (Addgene). The resultant vector was digested with AgeI and SphI to obtain a fragment containing loxP/lox2272 sequences for the FLEX switch, the open reading frame of mCherry, and the sequence encoding TLR2/4 microRNA, and this fragment was used to replace the open reading frame of GFP in pLV-PGK-GFP ([Åkerblom et al., 2013](#)) (a kind gift from Dr. Johan Jakobsson at Lund University). The resultant plasmid was named pLV-PGK-DIO-mCherry-TLR4miR-TLR2miR, and was used to generate the lentiviral vector expressing TLR2/4 microRNA and mCherry specifically in cells expressing Cre recombinase. For simultaneous knockdown of endogenous *Tlr2* and *Tlr4* in the N9 microglial cells (a kind gift from Dr. Makoto Tsuda at Kyushu University), the fragment encoding mCherry and TLR2/4 microRNA was obtained from pLV-PGK-DIO-mCherry-TLR4miR-TLR2miR by PCR and inserted between SphI and AgeI sites of pLV-PGK-Sph/Pst, a plasmid derived from pLV-PGK-GFP containing an additional multiple cloning site. Then, the fragment containing the PGK promoter and blasticidin-resistance gene (blasticidin S deaminase, bsd) was obtained from pLenti6.4/R4R2/V5-DEST (Life Technologies) and inserted into the KpnI site. The resultant plasmid was named pLV-PGK-mCherry-TLR4miR-TLR2miR-PGK-bsd, and was used to generate the lentiviral vector expressing TLR2/4 microRNA, mCherry and the blasticidin-resistance gene constitutively.

To generate a lentiviral vector expressing control microRNA, the DNA fragment encoding control microRNA (5'-TGC TGA AAT GTA CTG CGC GTG GAG ACG TTT TGG CCA CTG ACT GAC GTC TCC ACG CAG TAC ATT T-3' and 5'-CCT GAA ATG TAC TGC GTG GAG ACG TCA GTC AGT GGC CAA AAC GTC TCC ACG CGC AGT ACA TTT C-3'), which can form a hairpin structure processed into mature microRNA, but is predicted not to target any known vertebrate gene, was used instead of those encoding *Tlr2* microRNA and *Tlr4* microRNA. The resultant plasmid contains loxP/lox2272 sequences for the FLEX switch, the open reading frame of mCherry, and the sequences encoding two copies of control miRNA in tandem, and was used to generate the lentiviral vector expressing control miRNA and mCherry only in the presence of Cre recombinase.

A lentiviral vector expressing either a *Tlr2* or *Tlr4* synonymous mutant resistant to the respective miRNA simultaneously with TLR2/4 microRNA specifically in cells expressing Cre recombinase was generated as follows. The open reading frames of *Tlr2* and *Tlr4* attached with HA-tag and FLAG-tag at the C-terminals, respectively, were PCR-amplified from pCMV-SPORT-mTLR2 and pCMV-SPORT6-mTLR4 using primers containing sequences for the respective tags (for HA, 5'-TAT CCC TAT GAT GTG CCA GAC TAT GCT-3' and for FLAG, 5'-GAC TAC AAG GAT GAC GAT GAC AAG-3'). The amplified open reading frames were inserted between AgeI and SalI sites of pLV-PGK-Sph/Pst to generate pLV-PGK-TLR2-HA and pLV-PGK-TLR4-FLAG. Seven or 8 nucleotides within the microRNA-targeting regions of *Tlr2* and *Tlr4* in these plasmids were substituted without changing their amino acid sequences (see [Figures S6C](#) and [S6D](#)) by PCR to generate pLV-PGK-TLR2mt7-HA and pLV-PGK-TLR4mt8-FLAG, respectively. The open reading frames of the mutated *Tlr2* and *Tlr4* (TLR2mt7-HA and TLR4mt8-FLAG, respectively) were obtained from pLV-PGK-TLR2mt7-HA or pLV-PGK-TLR4mt8-FLAG by PCR and inserted between the Nhel and BssBI sites of pLV-PGK-DIO-mCherry-TLR2/4 miRNA to replace the open reading frame of mCherry in this plasmid. The resultant plasmids were named pLV-PGK-DIO-TLR2mt7-HA-TLR2/4 miRNA and pLV-PGK-DIO-TLR4mt8-FLAG-TLR2/4 miRNA.

Lentiviral vectors were produced as described previously ([Hioki et al., 2007](#)). The plasmids generated above and helper plasmids from a Lenti-X HTX packaging System (Clontech) were transfected into Lenti-X 293T cells (a derivative of HEK293T cells; Clontech) with Xfect Polymer (Clontech). At 8 h after transfection, the medium was replaced with virus production medium containing UltraCULTURE (Cambrex), 0.1 M MEM Non-Essential Amino Acids (NEAA; Life Technologies), 4 mM L-glutamine (Life Technologies), 2 mM GlutaMAX (Life Technologies) and 1 mM sodium pyruvate (Nacalai). The medium was collected at 48 h after transfection and concentrated with an Amicon Ultra-15 Centrifugal Filter Unit (Millipore). To determine the titer of the generated lentiviral vectors, genomic RNA was extracted from the lentiviral vectors and subjected to quantitative RT-PCR analysis using a Lenti-X qRT-PCR Titration Kit (Clontech).

Knockdown of TLR2/4 in cultured cells

Plasmids containing cDNA clones encoding mouse *Tlr1*, *Tlr2*, *Tlr3*, *Tlr4*, *Tlr5*, *Tlr6*, *Tlr7*, *Tlr8*, *Tlr9*, *Tlr11*, *Tlr12* and *Tlr13* were obtained from GE Dharmacon, Addgene, and R&D Systems. The plasmids containing mouse *Tlr1*, *Tlr2*, *Tlr4*, *Tlr6* and *Tlr9* have the CMV promoter, so that the respective genes are constitutively expressed. Since the other plasmids do not have any promoter sequence, the open reading frames of the respective genes were subcloned into pcDNA3.1 to generate the mammalian expression plasmids with a CMV promoter. To quantify the knockdown efficiency of TLR2/4 microRNA, both a TLR-expressing plasmid and a microRNA-expressing plasmid were transfected into Lenti-X 293T cells with Lipofectamine 2000 (Thermo Fisher Scientific). At 48 h after transfection, the cells were harvested to purify total RNA using a Nucleospin RNA kit (Macherey-Nagel). For simultaneous knockdown of endogenous *Tlr2* and *Tlr4* in the N9 microglial cells, the cells were infected with the lentivirus vector which expresses TLR2/4 microRNA, mCherry, and the blasticidin-resistance gene (pLV-PGK-mCherry-TLR4miR-TLR2miR-PGK-bsd). From the next day, the cells were incubated with blasticidin (final concentration; 5 μ g/ml) for two days. After blasticidin was removed, the cells were cultured for 4 days, and then harvested to purify total RNA. The specificity and efficiency of the knockdown were validated using quantitative RT-PCR, as described above.

Injection of lentiviral vectors into the mPFC

Under anesthesia with isoflurane, a lentiviral solution of 500 nL per injection site at 2×10^9 copies/ml was stereotactically pressure-injected at two sites in each hemisphere, bilaterally, into the mPFC using a PV-830 Pneumatic PicoPump (World Precision Instruments) through a glass micropipette made with a PN-30 micropipette puller (Narishige). The stereotaxic coordinates were targeted to the infralimbic cortex: 1.9 mm anterior from the bregma, 0.3 and 0.5 mm lateral from the midline, and 3.0 mm ventral from the skull surface at the bregma according to a mouse brain atlas (Paxinos and Franklin, 2003).

Transcriptome analyses

For transcriptome analysis in mPFC tissue, wild-type mice were subjected to R-SDS. At 4 h after the last stress exposure, mice were transcardially perfused with ice-cold D-PBS under deep anesthesia with i.p. injection of sodium pentobarbital. Brains were sliced at 0.5-mm intervals using a mouse brain slicer matrix. mPFC was collected in RNA Later (Life Technologies) using a 1.5 mm biopsy punch (Kai Industries). Total RNA was prepared using an RNeasy Plus Mini kit (QIAGEN). The resultant RNA (35 ng per array isolated from the mPFC of an individual mouse) was converted to cDNA using a Low Input Quick Amp Labeling Kit (Agilent Technologies). The cDNA samples were used to synthesize Cy3-labeled cRNA using a Low Input Quick Amp Labeling Kit (Agilent Technologies). The resultant Cy3-labeled cRNA was fragmented and hybridized with a SurePrint G3 Mouse GE 8 \times 60K Microarray (Agilent Technologies).

For mPFC microglia- or NAc microglia-specific transcriptome analyses, CX3CR1-EGFP mice and TLR-DKO mice were crossed to generate CX3CR1-EGFP mice lacking TLR2 and TLR4 (TLR-DKO; CX3CR1-EGFP mice). CX3CR1-EGFP mice and TLR-DKO; CX3CR1-EGFP mice were subjected to R-SDS. At 90 min after the last stress exposure, mice were transcardially perfused with ice-cold D-PBS under deep anesthesia with i.p. injection of sodium pentobarbital. Brains were sliced at 0.5-mm intervals using a mouse brain slicer matrix. The mPFC and NAc were collected using a 1.5 mm biopsy punch (Kai Industries). EGFP-positive cells were isolated as described above. To ensure that each sample had 500 pg of total RNA, which was sufficient for subsequent processing, microglia isolated from the mPFC or NAc of 3-6 mice were pooled for each sample. Total RNA was prepared using an RNeasy Plus Mini kit (QIAGEN). The resultant RNA was amplified and converted to cDNA using an Ovation RNA Amplification System V2 (NuGEN). The cDNA samples were used to synthesize Cy3-labeled cDNA using a SureTag DNA labeling kit (Agilent Technologies). The resultant Cy3-labeled cDNA was hybridized with a SurePrint G3 Mouse GE 8 \times 60K Microarray (Agilent Technologies).

Signal values were normalized to the average across all probes on each chip. Signals for a given probe were considered to be significantly different between two groups if the difference was larger than two-fold and significant for an unpaired t test at the 5% false positive rate. These analyses were performed using Gene Spring 12.6 (Agilent Technologies).

Local infusion of neutralizing antibodies into the mPFC

Under anesthesia with isoflurane, cannulas were implanted into the mPFC. The stereotaxic coordinates were targeted to the infralimbic cortex as described above. After a 7-day recovery, 1 μ L of PBS containing a mixture of neutralizing antibodies to IL-1 α (16-7011-85; eBioscience, RRID:AB_469199) and TNF α (506331; BioLegend, RRID:AB_11147367) (0.25 μ g each) per injection site was pressure-injected bilaterally into the mPFC using a microsyringe pump (Eicom). For a negative control, either or both of the two antibodies were replaced by the same amount of corresponding isotype antibodies (16-4888-85; eBioscience, RRID:AB_470172 and 400431; BioLegend, RRID:AB_11150233). At 2 h after the infusion, mice were subjected to a shorter version of R-SDS, followed by the social interaction test, as described above.

QUANTIFICATION AND STATISTICAL ANALYSIS

We did not exclude any samples (e.g., mice and neurons) from our statistical analyses. Data are shown as means \pm SEM. Comparison of two groups was analyzed by a two-sided unpaired t test, with Welch's correction if the assumption of equal variance was violated. For comparison of more than two groups, multiple comparison tests with Bonferroni correction were used. For correlative analyses, a Pearson correlation was performed. The analyses were performed with PRISM 7.0 software (GraphPad). *P* values less than 0.05 were considered to be significant. All the statistical details can be found in Table S1.

DATA AND SOFTWARE AVAILABILITY

The raw data have been deposited in the Mendeley Data under the following URL: <https://data.mendeley.com/datasets/2tyyncv6rm/1>.

The accession number for the DNA microarray data reported in this paper is GEO: GSE115996.

Supplemental Information

**The Innate Immune Receptors TLR2/4 Mediate
Repeated Social Defeat Stress-Induced Social
Avoidance through Prefrontal Microglial Activation**

Xiang Nie, Shiho Kitaoka, Kohei Tanaka, Eri Segi-Nishida, Yuki Imoto, Atsubumi Ogawa, Fumitake Nakano, Ayaka Tomohiro, Kazuki Nakayama, Masayuki Taniguchi, Yuko Mimori-Kiyosue, Akira Kakizuka, Shuh Narumiya, and Tomoyuki Furuyashiki

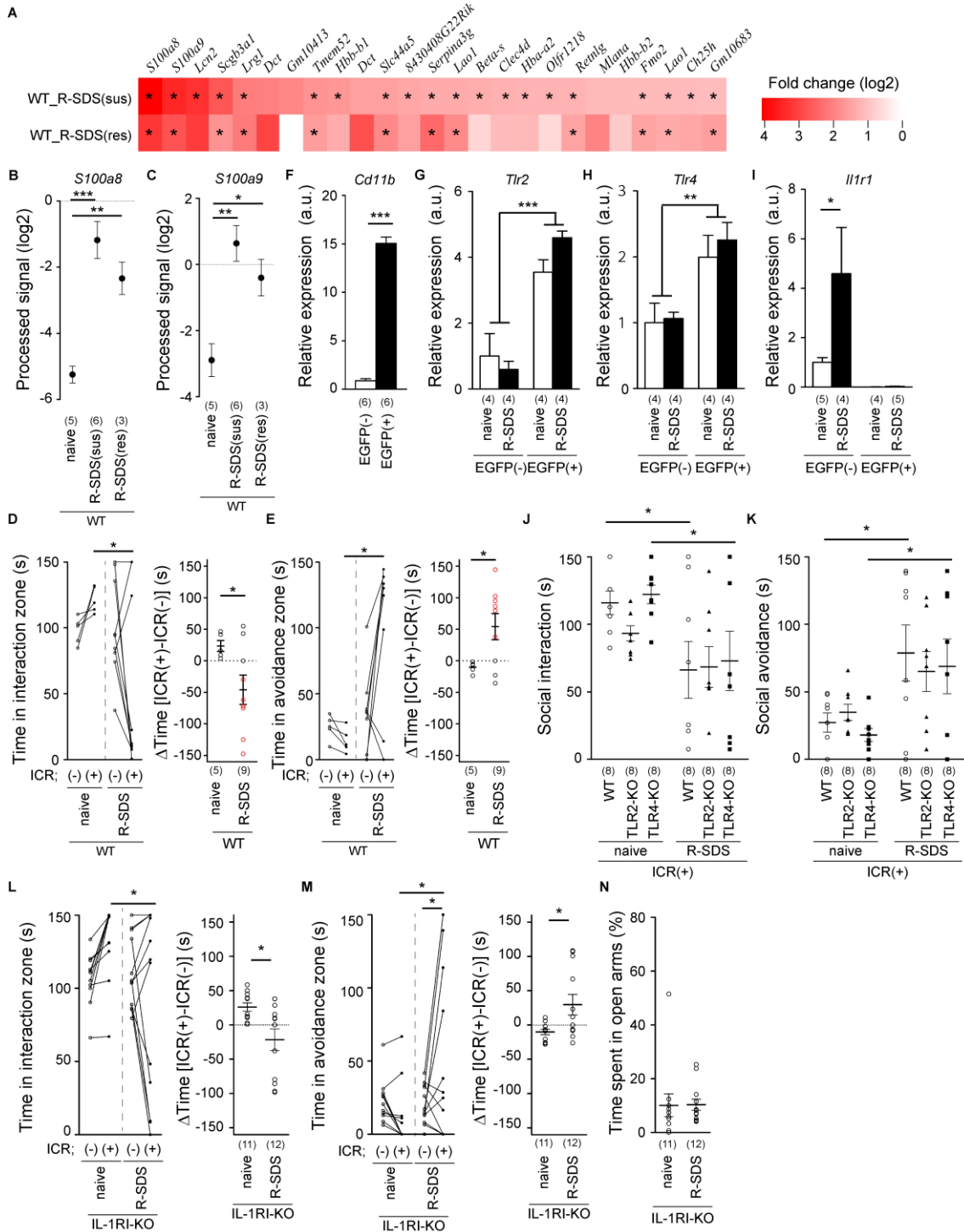


Figure S1, related to Figures 1 and 2.

Behavioral and gene expression analyses of TLR2, TLR4, and IL-1RI

(A) A heat map showing R-SDS-induced changes in gene expression of the top 25 most upregulated genes in the mPFC from susceptible and resilient wild-type mice (“WT_R-SDS(sus)” and “WT_R-SDS(res)”,

respectively). * $P<0.05$ for unpaired *t*-test for the changes in gene expression for the indicated probes. **(B** and **C**) The expression levels of S100A8 (**B**) and S100A9 (**C**) in the mPFC of susceptible and resilient wild-type mice (“R-SDS(sus)” and “R-SDS(res)”, respectively) at 4 h after R-SDS as well as wild-type mice without SDS (“naïve”). * $P<0.05$, ** $P<0.01$, *** $P<0.001$ for Bonferroni’s multiple comparison test. **(D** and **E**) The durations for presence in the interaction (**D**) or avoidance (**E**) zone without and with an ICR mouse and the differences between these durations without and with an ICR mouse (Δ Time [ICR(+)-ICR(-)]), for wild-type mice (“WT”) with or without prior R-SDS (“R-SDS” and “naïve”). Red dots in right panels indicate the data from susceptible mice. * $P<0.05$ for Bonferroni’s multiple comparison test (left panels) or unpaired *t*-test (right panels). **(F-I)** mRNA levels of CD11b (**F**), TLR2 (**G**), TLR4 (**H**) and IL-1RI (**I**) in EGFP-positive cells (“EGFP(+)”) and EGFP-negative cells (“EGFP(-)”) isolated from CX3CR1-EGFP mice, in which EGFP is selectively expressed in microglia and monocytes (a minor population) in the brain, with or without prior R-SDS (“R-SDS” or “naïve”, respectively). The levels were normalized to that of β -actin to minimize sample variance. The levels were further normalized to those of the control groups, namely EGFP(-) in Figure S1F and naïve EGFP(-) in Figure S1G-I, and are shown. *** $P<0.001$ for unpaired *t*-test (**F**) and * $P<0.05$ for Bonferroni’s multiple comparison test (**I**). **(J** and **K**) The durations for presence in the interaction (**J**) or avoidance (**K**) zone with an ICR mouse for wild-type mice (WT), TLR2-KO mice, and TLR4-KO mice before and after R-SDS (“naïve” and “R-SDS”, respectively). The same individuals were analyzed and statistically compared before and after R-SDS. * $P<0.05$ for Bonferroni’s multiple comparison test. **(L** and **M**) The durations within the interaction (**L**) or avoidance (**M**) zone without and with an ICR mouse and the differences between these durations without and with an ICR mouse (Δ Time [ICR(+)-ICR(-)]) in IL-1RI-KO mice with or without prior R-SDS (“R-SDS” or “naïve”, respectively). * $P<0.05$ for Bonferroni’s multiple comparison test (left panels) or unpaired *t*-test (right panels). **(N)** The level of anxiety of IL-1RI-KO mice with or without prior R-SDS (“R-SDS” or “naïve”, respectively). The proportion of the time spent in the open arms in the elevated plus maze was measured as an index of anxiety. The number of mice is shown below each group. Data are shown as means \pm SEM.

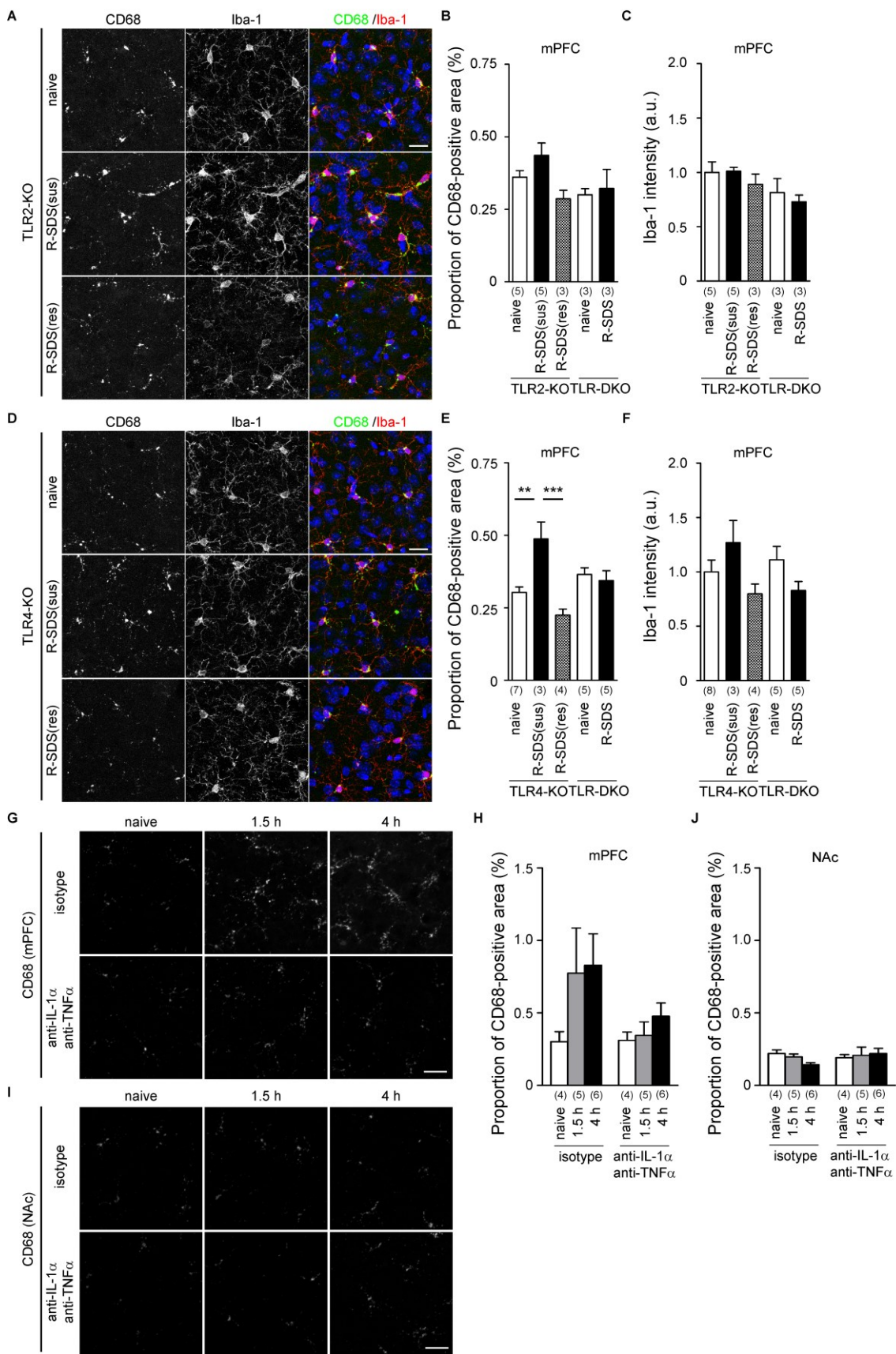


Figure S2, related to Figures 3 and 8.

TLR2 and TLR4 deficiency attenuates R-SDS-induced activation of mPFC microglia

(A-F) Representative images (A and D) and quantitative analyses (B, C, E and F) of immunostaining for CD68 and Iba-1 in the mPFC of TLR2-KO mice (A-C) and TLR4-KO mice (D-F) without SDS (“naïve”), susceptible and resilient mice (“R-SDS(sus)” and R-SDS(res)”, respectively) with the respective genotypes, and TLR-DKO littermates (B, C, E and F) with or without R-SDS (“R-SDS” and “naïve”, respectively) at 1.5 h after the last session of R-SDS. The images from TLR-DKO littermates are not shown in this figure, since these images are similar to those from TLR-DKO mice shown in Figure 3A and 3C. In the merged images, CD68 and Iba-1 signals are shown in green and red, respectively. CD68 signals in Iba-1 positive microglia are seen in yellow. Nuclei were counterstained with Hoechst 33342 and are shown in blue. The values of Iba-1 intensity were normalized to that of naïve TLR2-KO or TLR4-KO mice for Figure S2C or S2F, respectively. (G-J) Representative images (G and I) and quantitative analyses (H and J) of immunostaining of CD68 in the mPFC (G and H) and NAc (I and J) of wild-type mice which received mPFC infusions with a mixture of neutralizing antibodies for IL-1 α and TNF α (“anti-IL-1 α anti-TNF α ”) or control antibodies of the corresponding isotypes (“isotype”) without SDS (“naïve”), and at 1.5 h and 4 h after the last session of a shorter version of R-SDS (see Figure 8A). Scale bars, 20 μ m. ** P <0.01, *** P <0.001 for Bonferroni’s multiple comparison test. The number of mice is shown below each group. Data are shown as means \pm SEM.

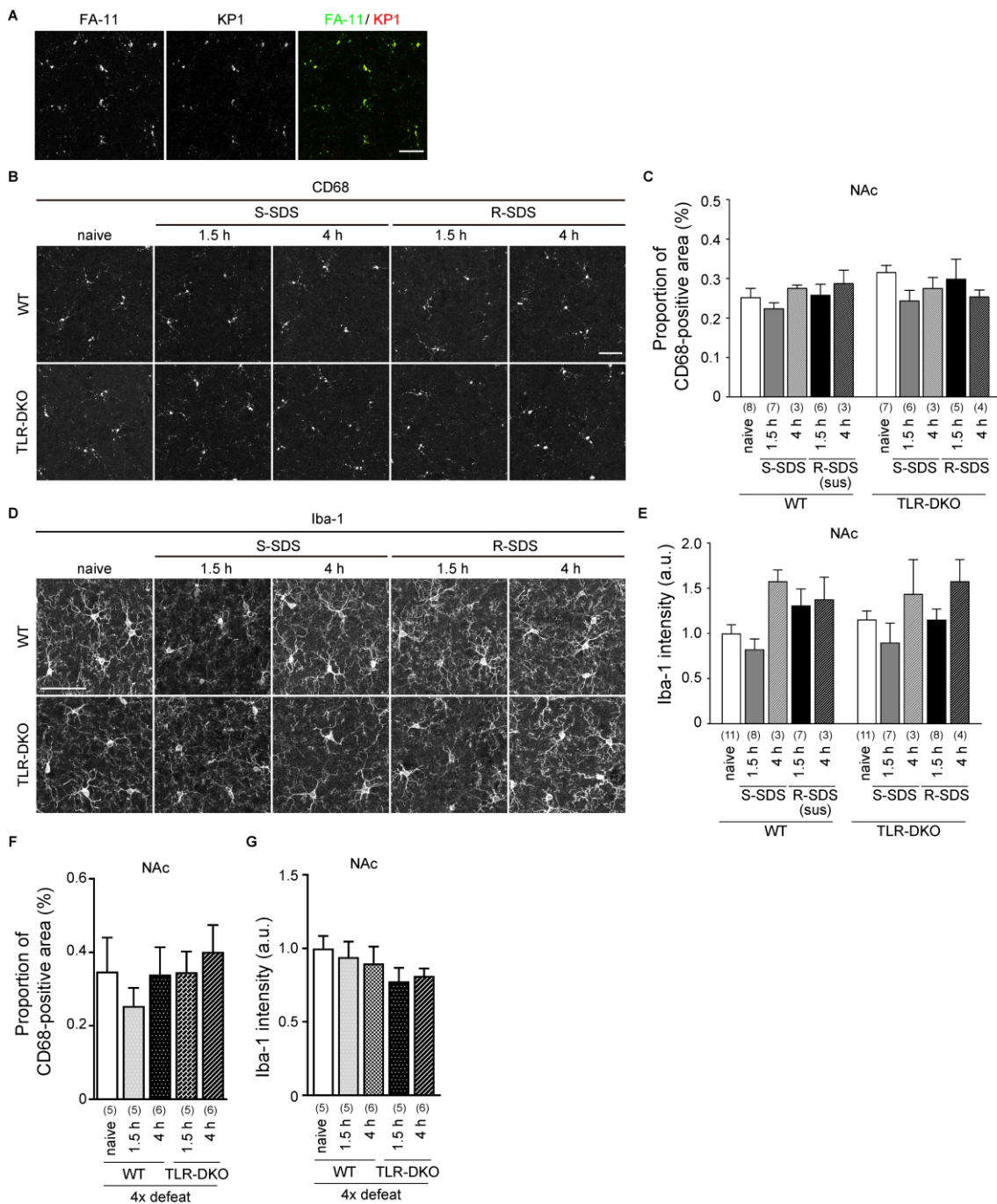


Figure S3, related to Figure 3.

R-SDS does not induce activation of NAc microglia in wild-type mice or TLR-DKO mice

(A) Colocalization of CD68 signals with FA-11, a monoclonal anti-CD68 antibody which was mainly used in this study, and those with KP1, another monoclonal anti-CD68 antibody. This colocalization with the two independent antibodies confirmed the specificity of CD68 signals. Scale bar, 50 μ m. **(B-E)** Representative images (**B** and **D**) and quantitative analyses (**C** and **E**) of CD68 (**B** and **C**) and Iba-1 (**D** and

E) immunostaining in the NAc of wild-type mice (WT) and TLR-DKO mice without SDS (“naïve”), and at 1.5 h and 4 h after S-SDS and the last session of R-SDS. For wild-type mice after R-SDS, the images were taken and analyzed only from susceptible mice (“R-SDS(sus)”). Scale bars, 50 μ m. (**F** and **G**) Quantitative analyses of CD68 (**F**) and Iba-1 (**G**) immunostaining in the NAc of wild-type mice (WT) and TLR-DKO mice without SDS (“naïve”) and at 1.5 h and 4 h after the last session of R-SDS for 4 days (“4 \times defeat”). The values of Iba-1 intensity were normalized to that of naïve wild-type mice. The number of mice is shown below each group. Data are shown as means \pm SEM.

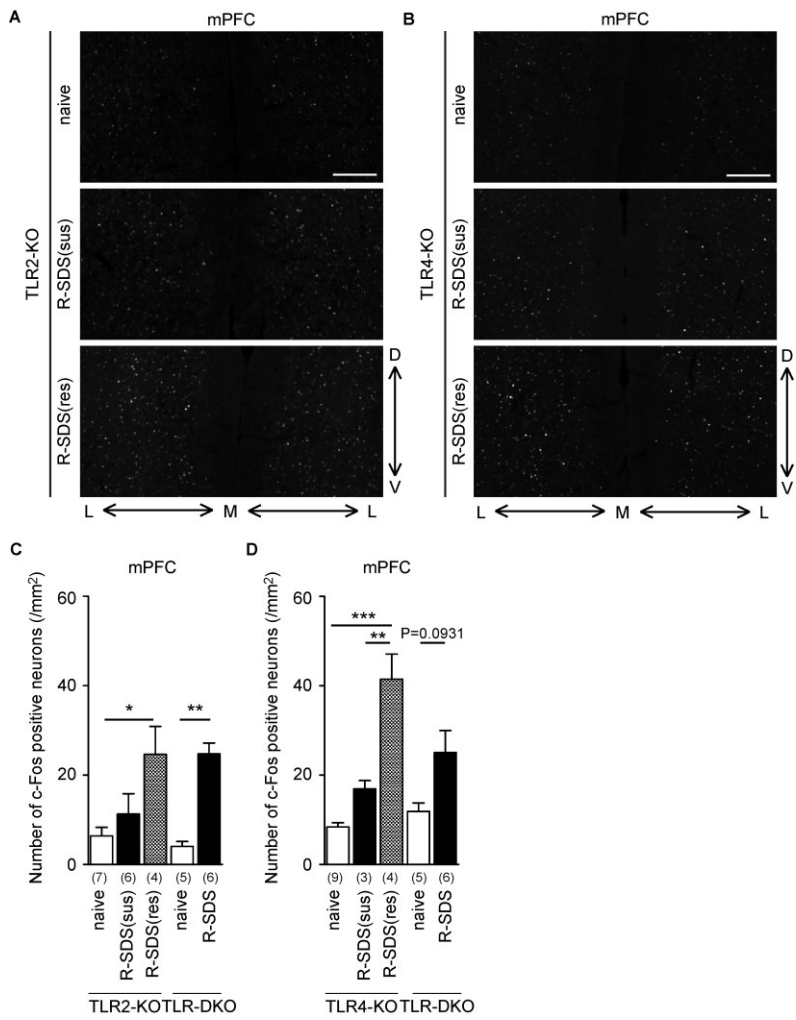


Figure S4, related to Figure 5.

SDS-induced c-Fos expression in mPFC neurons of TLR2-KO mice and TLR4-KO mice as well as TLR-DKO littermates

Representative images (A and B) and quantitative analyses (C and D) of c-Fos immunostaining in mPFC of TLR2-KO mice (A and C) and TLR4-KO mice (B and D) without SDS (“naïve”), susceptible and resilient mice (“R-SDS(sus)” and “R-SDS(res)”, respectively) of the respective genotypes, and TLR-DKO mice (C and D) with or without R-SDS (“R-SDS” and “naïve”, respectively) at 1.5 h after the last session of R-SDS. The images from TLR-DKO littermates are not shown in this figure, since these images are similar to those from TLR-DKO mice shown in Figure 5B. The orientations of the images are indicated by arrows (L, lateral; M, medial; D, dorsal; V, ventral). Scale bars, 100 μm . * $P<0.05$, ** $P<0.01$, *** $P<0.001$ for Bonferroni’s multiple comparison test. The number of mice is shown below each group. Data are shown as means \pm SEM.

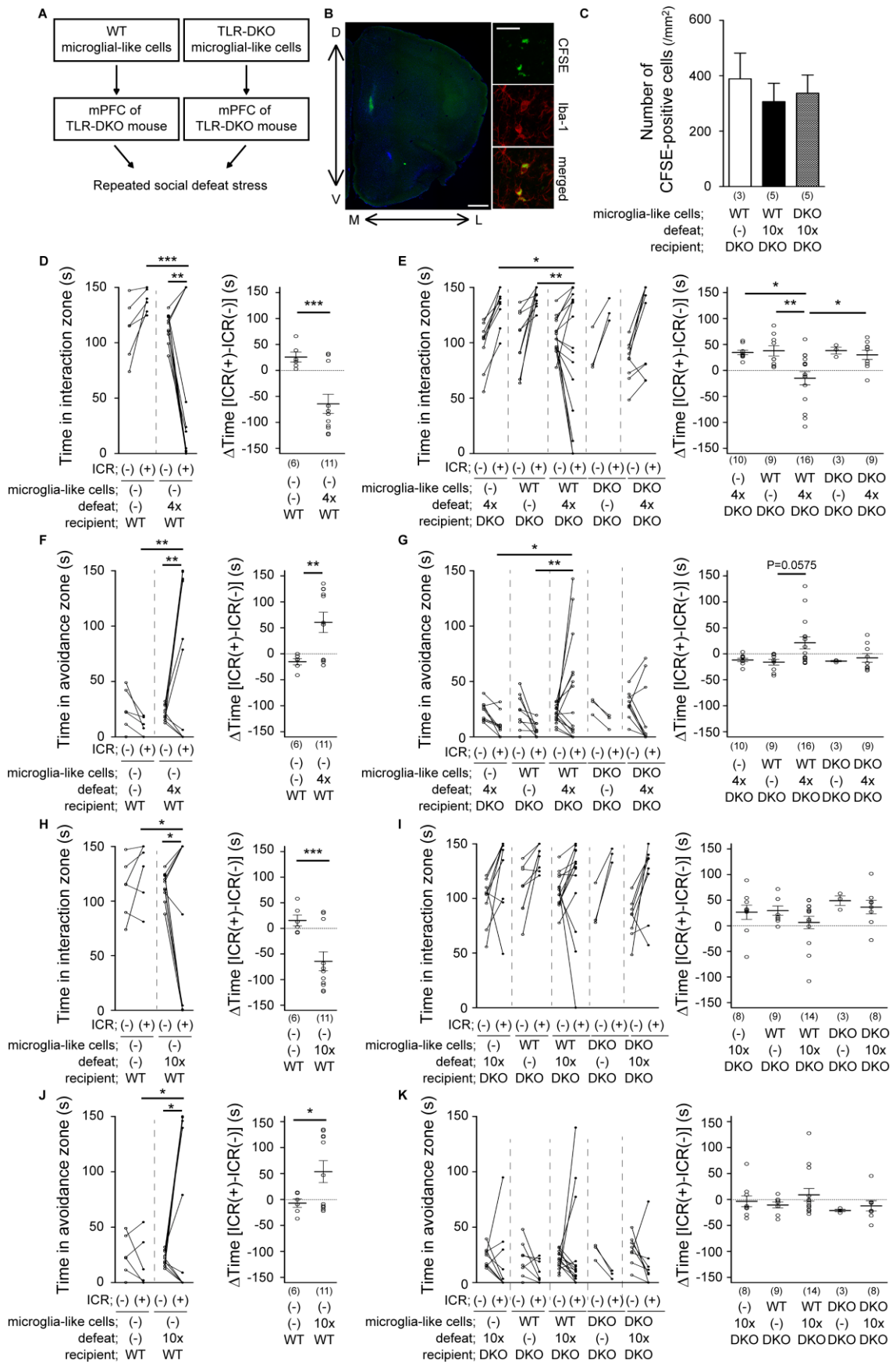


Figure S5, related to Figure 6.

Transplantation of wild-type microglia-like cells into the mPFC of TLR-DKO mice transiently restores social avoidance induced by R-SDS

(A) Design of behavioral experiments with transplantation of microglia-like cells. Primary microglia-like cells were obtained from wild-type (WT) and TLR-DKO neonates, and were transplanted to the mPFC of TLR-DKO mice. After a four-week recovery, the mice were subjected to R-SDS. (B) Representative images of transplanted microglia-like cells in the mPFC. Wild-type microglia-like cells were labeled with CFSE and locally infused into the mPFC of TLR-DKO mice. Fluorescence images were taken after the four-week recovery. Microglia were visualized by Iba-1 staining. CFSE and Iba-1 signals are shown in green and red, respectively. Nuclei counterstained with Hoechst 33342 are shown in blue. The orientations of the images are indicated by arrows (L, lateral; M, medial; D, dorsal; V, ventral). Scale bars, 500 μ m and 25 μ m for the lower and higher magnifications, respectively. (C) The numbers of CFSE-positive cells in TLR-DKO mice that received transplantation of wild-type (WT) or TLR-DKO (DKO) microglia-like cells into the mPFC with or without prior R-SDS for 10 days (“10 \times ” or “(-)”, respectively). (D-K) The durations for presence in the interaction (D, E, H and I) or avoidance (F, G, J and K) zone without and with an ICR mouse and the differences between these durations without and with an ICR mouse (Δ Time [ICR(+)-ICR(-)]) in wild-type recipient mice (WT) that received a sham operation (“(-)”) (D, F, H and J), and in TLR-DKO recipient mice which received a sham operation (“(-”), or transplantation of wild-type (WT) or TLR-DKO (DKO) microglia-like cells into the mPFC (E, G, I and K) with or without prior R-SDS for 4 days (“4 \times ” or “(-”), respectively; D-G) or for 10 days (“10 \times ” or “(-”, respectively; H-K). n.s. (not significant), * $P<0.05$, ** $P<0.01$, *** $P<0.001$ for unpaired t -test for pairwise comparisons, or for Bonferroni’s multiple comparison test for comparisons among more than two groups. The number of mice is shown below each group. Data are shown as means \pm SEM.

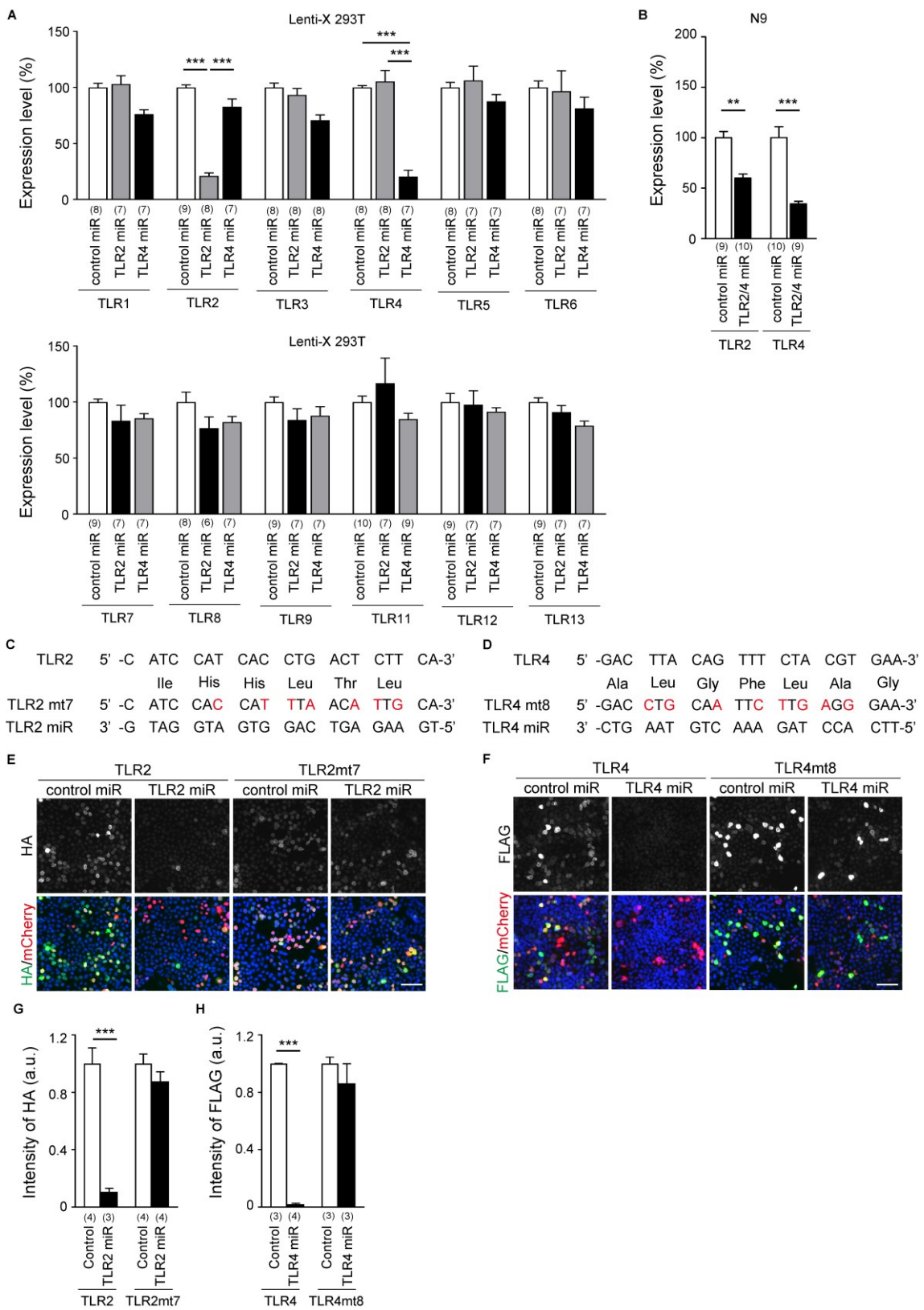


Figure S6, related to Figure 6.

TLR2/4 microRNA selectively suppresses mRNA expression of TLR2 and TLR4 *in vitro*

(A) RNA interference with TLR2 or TLR4 microRNA efficiently and specifically suppresses mRNA expression of the corresponding TLR isoform in Lenti-X 293T cells. Various mouse TLR isoforms (TLR1 to TLR13) were overexpressed with TLR2 or TLR4 microRNA (miR) as well as control microRNA, and their expression levels were quantified by real-time RT-PCR. *** $P<0.001$ for Bonferroni's multiple comparison test. (B) Lentivirus-delivered TLR2/4 microRNA, in which TLR4 microRNA and TLR2 microRNA are tandemly connected, simultaneously suppressed endogenous mRNA expression of TLR2 and TLR4 in the N9 microglial cells. The values were normalized to those with control microRNA. ** $P<0.01$, *** $P<0.001$ for unpaired *t*-test. (C and D) DNA sequences for microRNA-targeting regions of TLR2 (C) and TLR4 (D) and the corresponding regions of microRNA-resistant mutant cDNAs of these genes ("TLR2mt7" and "TLR4mt8", respectively) with no change in the amino acid sequences. Mutations in these mutants are highlighted in red. (E and F) Representative images of immunostaining for TLR2 (E), TLR4 (F) or the respective microRNA-resistant mutants ("TLR2mt7" and "TLR4mt8") with the corresponding microRNA or control microRNA in Lenti-X 293T cells. TLR2 and TLR2mt7 cDNAs were tagged with HA and detected by HA immunostaining. TLR4 and TLR4mt8 cDNAs were tagged with FLAG and detected by FLAG immunostaining. mCherry was simultaneously expressed with TLR2 or TLR4 microRNA to identify cells expressing these miRNAs. HA or FLAG signals and mCherry are shown in green and red, respectively, in the merged images. Nuclear counterstaining with Hoechst 33342 is shown in blue. Scale bars, 25 μ m. (G and H) The fluorescent intensities of HA (G) and FLAG (H) tags in the experimental conditions shown in E and F, respectively. The values were normalized to those with control microRNA. *** $P<0.001$ for unpaired *t*-test. The number of analyzed wells is shown below each group. Data are shown as means \pm SEM.

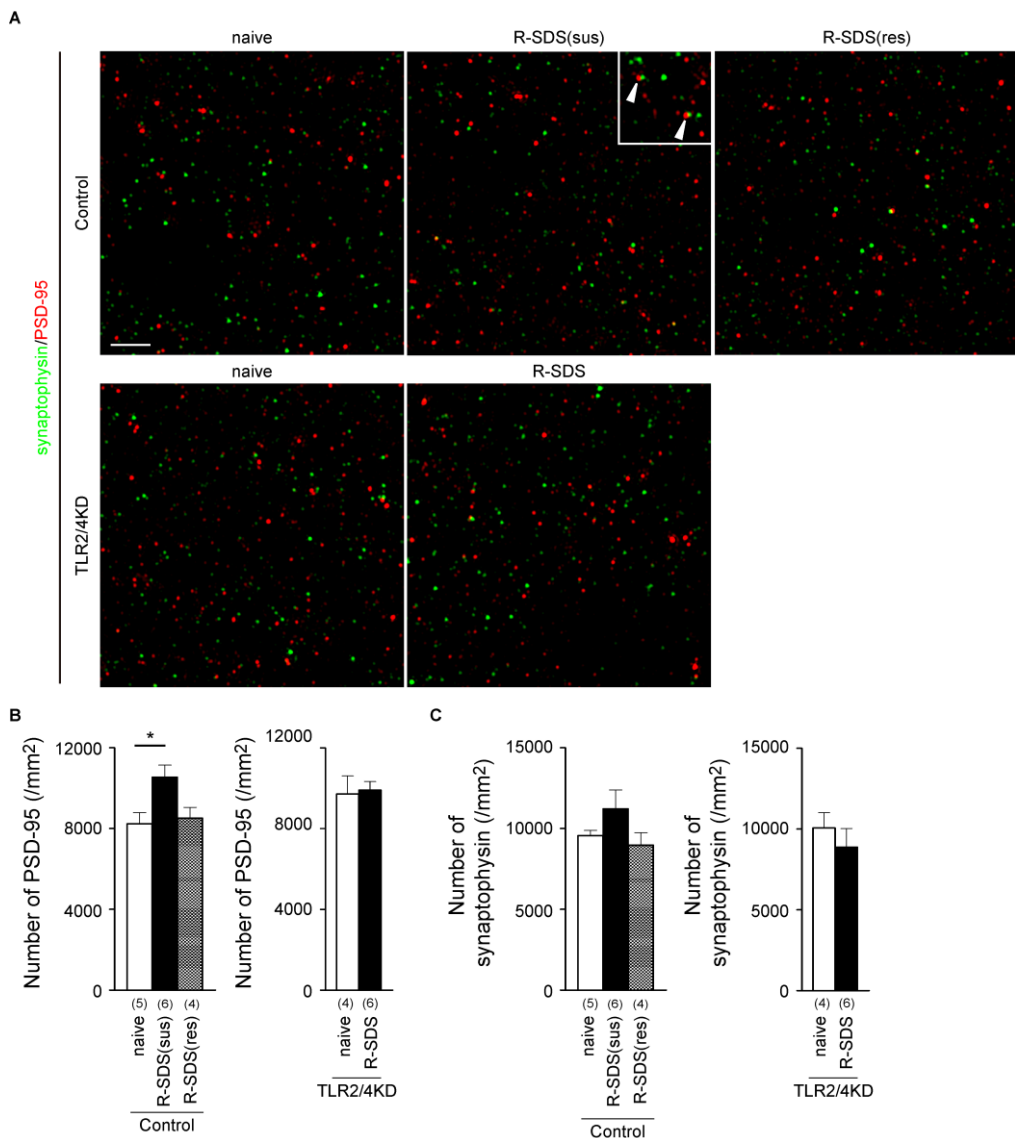


Figure S7, related to Figure 6.

R-SDS increases the number of PSD-95-positive puncta in the mPFC in a manner dependent on TLR2/4 expressed in mPFC microglia

Representative SIM images (A) and quantitative analyses (B and C) of immunostaining for synaptophysin (green in A) and PSD-95 (red in A) in the deep layer of the mPFC of CX3CR1-CreER mice that received mPFC injections of lentiviral vectors expressing control microRNA (“Control”) or TLR2/4 microRNA (“TLR2/4KD”). The images were taken from susceptible and resilient CX3CR1-CreER mice (“R-SDS(sus)”) and (“R-SDS(res)”, respectively) expressing control microRNA, and those expressing TLR2/4 microRNA (“R-SDS”) at 1.5 h after R-SDS, as well as those expressing control or TLR2/4 microRNA without R-SDS (“naïve”). Arrowheads in A indicate the juxtaposition of synaptophysin and PSD-95 punctate signals reminiscent of excitatory synapses. Scale bar, 5 μm . * $P<0.05$ for Bonferroni’s multiple comparison test.

The number of mice is shown below each group. Data are shown as means \pm SEM.

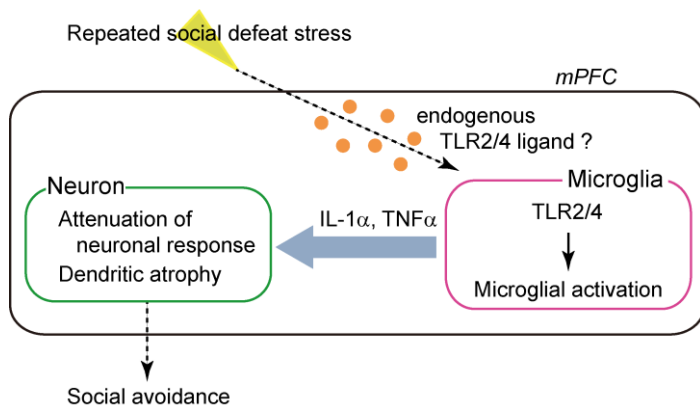


Figure S8, related to all Figures.

The role of TLR2/4 in mPFC microglia for R-SDS-induced neuronal and behavioral changes

Our findings demonstrate that R-SDS induces activation of mPFC microglia through TLR2/4 for neuronal and behavioral changes, although the endogenous TLR2/4 ligand for this microglial activation remains to be identified. We also suggest that IL-1 α and TNF α derived from the activated mPFC microglia mediate neuronal response attenuation and dendritic atrophy in the mPFC, thereby leading to social avoidance.